MASTER

PREPRINT UCRL- 79788

CONF-771136-27

Lawrence Livermore Laboratory

A SIMPLE SCALING MODEL FOR EXPLODING PUSHER TARGETS

E. K. Storm, J. T. Larsen, J. H. Nuckolls, H. G. Ahlstrom and K. R. Manes

November 4, 1977

This paper was prepared for submission to the APS Plasma Physics Meeting of the American Physical Society, Atlanta, Georgia, November 5-11, 1977.

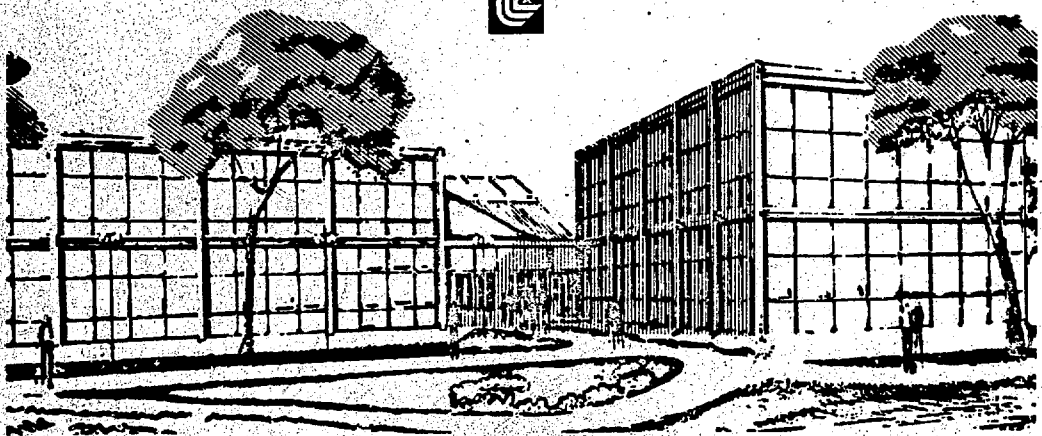

A SIMPLE SCALING MODEL FOR EXPLODING PUSHER TARGETS

E. K. Storm, J. T. Larsen

J. H. Nuckolls, H. G. Ahlstrom, and K. R. Manes

Abstract Submitted

for the APS Plasma Physics Meeting of the

American Physical Society

November 5-11, 1977

Physics and Astronomy
Classification Scheme
Number 52

Bulletin Subject Heading in which Paper should be placed
Inertial Confinement, Lasers, Pellet Simulation, Design and Experiments

A Simple Model for Exploding Pusher Targets.

E.K. Storm, J.T. Larsen, J.H. Nuckolls, H.G. Ahlstrom and K.R. Manes, Lawrence Livermore Laboratory.**

A simple model has been developed, which when normalized by experiment or Lasnex calculations can be used to scale neutron yields for variations in laser input power and pulse length and target radius and wall thickness. The model also illucidates some of the physical processes occuring in this regime of laser fusion experiments. Within certain limitations on incident intensity and target geometry, the model scales with experiments and calculations to within a factor of two over six decades in neutron yield.

**Supported by U. S. ERDA Contract W-7405-ENG-48

Submitted by

Erik K. Storm

Erik K. Storm
University of California
Lawrence Livermore Laboratory
P. O. Box 808, L-549
Livermore, CA 94550

I. INTRODUCTION

A laser irradiated target is said to operate in an exploding pusher mode[1,2] when the pusher significantly decompresses in the process of compressing and heating the fuel. The exploding pusher mode is characterized by a high rate of energy addition to the pusher which causes a near supersonic thermal wave[3] to propagate through the pusher prior to any significant compression. Multiple shock compressions of the fuel and heat addition by electron thermal conduction from the laser absorption region, produce a large entropy change in the fuel at early times.[4-7] Even though the later stages of the implosion appear to be nearly isentropic[4-7] (partly due to the long electron-ion equilibration times) this early entropy change results in a limited fuel density increase.

For the ideal laser driven exploding pusher target experiment one-half of the pusher mass (in our case, the SiO_2 microshell surrounding the DT fuel) implodes inward to compress and heat the fuel and the remaining one-half of the pusher mass expandes outward. This is in contrast to the ablatively driven target where a large fraction of the shell mass is ablated during the implosion to produce the compression of the pusher and fuel.[8] The ratio of the actual length of the applied laser pulse to a characteristic hydrodynamic implosion time scale* and the question of preheat versus nearly isentropic compression, is more related to the efficiency of the process and the relative success of any specific target design, than to the distinction between exploding pusher and an ablatively driven target. Clearly, if the laser pulse, or equivalently, the heating of the glass shell occurs in effectively zero time (say less than a few picoseconds) the shell will explode in a manner appropriate to the definition of an exploding pusher given above. Conversely, it is quite possible to have a laser pulse of Gaussian temporal shape, whose

*[defined as the time from when the inward moving portion of the pusher has acquired 10% of its peak velocity, until the pusher stagnates at peak compression]

FWHM is 2-3 times longer than the hydrodynamic implosion time scale, and still have the target operate as an exploding pusher. Two important issues for a target to operate in a near optimum exploding pusher mode, are the rate of energy deposition prior to any significant motion of the pusher/fuel interface, and proper matching of the pusher shell thickness to the superthermal electron mean free path.[7] The determination of optimum target geometry parameters and the fraction of the absorbed laser energy which contributes to the inward portion of the pusher and the heating of the fuel, is a central issue in exploding pusher scaling.

One of the more sensitive indications of target performance is the thermonuclear yield. In order to optimize the target performance for a given laser and target regime, numerous 1-D Lasnex[9] simulations are in general required, each of which requires several minutes of CDC 7600 computing time. It is clearly desirable to have a simple set of model equations to investigate the trends within the laser/target parameter space. As shown in Ref. 10, our experimental results from DT filled SiO_2 microshells irradiated with 1.06 um laser pulses, indicated that the neutron yield could be scaled with a fraction of the absorbed specific energy. This fraction was related to the ratio of the fluid dynamics implosion time to the laser pulse FWHM. This paper represents improvements and refinements of this concept and the development of a set of simple model equations which can be used to calculate the performance of exploding pusher targets in the vicinity of their optimum performance point. This includes a more realistic treatment for the compression than was proposed in that report and a treatment of the target performance as a function of the initial DT fill. Results from detailed Lasnex calculations[4-6] were used extensively as justification for otherwise intuitive physical reasoning. Part II of this paper briefly summarizes the pertinent experimental and calculational results for exploding pusher targets. In part III we derive the simple model equations while Part IV compares the model to our experimental results[10-21] and Lasnex 1-D simulations, respectively. Part V discusses some of the limitations of the model.

II. EXPLODING PUSHER BEHAVIOR

Figure 1 gives typical laser and target parameters and the experimental results for a high power, high yield exploding pusher target experiment.

Similar targets irradiated at power levels from 0.2 to 4.5 TW using focusing optics from approximately f/0.07 to f/2.5 have produced a rather complete experimental picture of the salient features of this type of experiment.[10-25] Both from these references, and from Lasnex 1-D simulations,[4-7] we can extract the following main events, or characteristic features of exploding pusher target behavior.*

(i) Self steepening of the density profile[24-25] and measurements of the plasma and the scattered 1.06 um light distributions[24] indicate that absorption is predominantly due to resonance absorption.[23,26,27] This, in conjunction with plasma instabilities, results in a strong superthermal component in the laser heated electron spectrum. Evidence for this superthermal component can be seen in the typical exploding pusher x-ray spectra shown in Figure 2.

(ii) During the early part of the pulse, before the high thermal pressure in the pusher causes it to explode,** these superthermal electrons penetrate the glass shell and the fuel, depositing some of

*Specific calculated values are for a Lasnex 1-D simulation performed for a 0.45 TW, 50 ps (FWHM, Gaussian shape), 1.06 μm laser pulse focused on a 70 μm diameter SiO_2 microschell with a 0.4 μm thick wall and filled with an equimolar mixture of DT at 2 mg/cc. The target achieved an average final compression ratio of approximately 75, a peak DT ion temperature of approximately 3.5 keV which produced 1.1×10^8 thermonuclear neutrons.

**To avoid semantic difficulties with the word explode, we define the explosion condition as the point in time when the shockwave breaks through the pusher causing a significant change in the accelleration of the inward moving pusher/fuel interface. For the simulation mentioned, for example, the accelleration increased by a factor of $\sim$ 100 to a value of $\sim 10^{18}$ cm/sec^2 over a period of $\sim$ 20 psec. raising the pusher/fuel interface velocity to 0.8×10^7 cm/sec approximately 45 psec before the peak of the pulse.

their kinetic energy in the shell and the fuel. Although the amount of energy deposited in the shell is insignificant compared with the total energy absorbed (~0.5 mJ vs approximately 5 J), the role played by the superthermal electrons is believed to be an extremely important one. In fact, Lasnex simulations run without the presence of super thermal electrons show the targets behaving more in the ablative mode and fail to reproduce agreement with experimental results.

(iii) Electron thermal conduction, driven by the absorption of the laser light near the critical density of the plasma, generates a thermal wave[3,29] propagating at near supersonic speeds through the pusher, driving a shockwave along with it. Lasnex simulations do not indicate a steep thermal front in the ideal self-similar form discussed in reference 3. It is more likely that the few eV temperature already existing in the shell and the temperature rise caused by the shockwave running through the shell, causes the thermal conduction front to be in the transition region between the linear and non-linear regime. As the shockwave breaks through the shell, and propagates through the fuel, the pusher explodes.

(iv) For the calculation quoted, the shell "jumps-off" with an initial velocity of $\sim 0.8 \times 10^7$ cm/sec and the pusher/fuel interface has moved in about 3% of the initial radius at this time. The pusher continues to "explode", driven by thermal conduction from the critical density region.

(v) The exploding pusher generatesa moderately strong shockwave of the order of a few megabars. Clearly as long as continuum fluid mechanics are valid, the rapidly accelerating pusher (driven by thermal conduction) acts as a piston driving a shockwave into the fuel.

(vi) The peak of the laser pulse has not yet been reached, and the inward moving pusher continues to be heated by laser driven electrons and accelerates to higher velocities.

(vii) When the pusher in the simulation quoted, has moved in approximately 35% of the initial radius, it has reached it's peak velocity and the remaining process appears to be essentially uncoupled from the "external world," as truncating the laser pulse in the 1-D simulation does not severely affect the target performance as measured by the neutron yield and the pusher/fuel interface trajectory.

(viii) The fuel ion temperature and density now primarily increase due to the compressive work done on the fuel by the imploding pusher. The post strong-shock compression heating is moderately isentropic, with an effective γ of 1.5-2.

(ix) The implosion culminates when the inner edge of the inward moving pusher stagnates against the compressed DT and converts its kinetic energy to thermal energy of the stagnated pusher and fuel. For the simulation quoted, this resulted in a compression of the order of 75 and peak DT ion temperatures of $\sim$ 3.5 keV.

(x) To a first approximation, the inner part of the imploded portion of the shell surrounding the DT fuel is in thermal equilibrium with the DT fuel at peak compression.

(xi) Also, to a first approximation, simulations show that the compressed DT density is proportional to the density obtained by filing the original shell volume by the imploding fraction ($\sim$ 1/2) of the shell mass

Lasnex, being a hydrodynamic code, gives by definition, a continuum description of heating and compression following the initial explosion phase. It should be mentioned that for sufficiently high initial pusher velocities ($\geq 4 \times 10^7$ cm/sec) and sufficiently low initial fuel densities ($\geq$ 0.5 mg/cc) the range of the DT ions produced by collisions with the imploding Si or O

ions approach the dimensions of the initial target radius. For these conditions ion-ion collisions in the DT fuel no longer generate an inward moving ion shock, and the continuum approach would clearly have to be treated with some caution. For the parameter regimes under discussion of this paper, however, and indeed for all of the exploding pusher experiments performed at LLL[10-25], we believe that continuum physics gives both an adequate and basically correct description of the phenomenon.

An example of the Lasnex 1-D simulation mentioned earlier is shown in figure 3. Here is displayed the pusher/fuel interface velocity and position as a function of time, with the Gaussian input laser pulse shown for time reference. Also shown are the interface velocity and trajectory with the corresponding reduction in neutron yield that results when the input pulse is truncated at the times indicated. During the early part of the pulse, the velocity is seen to increase rapidly from 0 to $\sim 0.8 \times 10^7$ cm/sec by about 45 psec before the peak of the pulse, without any significant inward translation, with the pusher/fuel interface having moved in ~ 0.7 μm, or approximately twice the initial pusher wall thickness. The interface is then seen to accelerate steadily until shortly after the peak of the laser pulse. In order to estimate how much of the laser input energy was "useful" as far as target performance is concerned, the Gaussian input pulse was truncated at the times (t_1-t_4) indicated, and the calculation allowed to continue. Clearly, truncating the input pulse at times greater than t_3 does not affect the performance at all, whereas truncating at times less than t_1 has a severe effect both on the fuel interface trajectory and the target performance as measured by the neutron yield. Truncating the pulse between t_1 and t_3 produces between 40 and 80% of the maximum neutron yield. This is demonstrated in figure 4 which shows the ratio of the actual to the maximum neutron yield, and the pusher/fuel interface as a function of different "cut-off" times. From this figure we see that truncating the laser pulse when the pusher/fuel interface has moved in $\sim$ 32% of the initial radius, produces 2/3 of the maximum neutron yield. Defining this "knee" on the curve as the transition point when the target appears to be uncoupled from further

absorption of the laser light, we arrive at a criterion for determining the useful fraction of the absorbed energy as that fraction of the energy absorbed until $t = t_c$. Clearly any energy absorbed after the target has reached stagnation, is not useful for producing thermonuclear reactions. Figures 3 and 4 and the discussion in this section suggests that a more sensitive measure of the "cut-off" condition is at a somewhat earlier point in time. This is clearly associated with the finite time required for information from the absorption region near the critical density to be transmitted to the pusher/fuel interface region.

In order to give some confidence to the interface velocity and trajectory histories shown in figures 3 and 4, and the implications derived from them, figures 5 and 6 compares Lasnex calculations to experimentally observed trajectories and velocities. These experiments were part of a series of experiments[14,16] performed on the Janus laser utilizing a near 4π illumination system[30], similar to the one employed by KMSF in their experiments.[31,32] The pusher/fuel interface trajectory was constructed by imaging the x-ray emission from an exploding pusher onto a 15 psec resolution x-ray streak camera[16,17]. The general qualitative agreement of the data in figure 5 and the Lasnex calculation is adequate. The data in figure 6 was obtained by employing a computer generated "ridge finding"[12] technique to the r-t x-ray data from a target illuminated from one side. This technique locates the instantaneous position of the maximum emission region as a function of position and time. Identifying this "ridge" as the pusher/fuel interface, allowed the derivative of the r-t diagram to be accurately determined. Since the Lasnex simulation was for a two sided, i.e. spherically symmetric illumination experiment, the data can only be compared to the simulation prior to the significant deceleration as the pusher stagnates in the center. With that limitation, the agreement between experiment and simulation, must again be said to be satisfactory.

III. DERIVATION OF THE SIMPLE MODEL.

Based upon the discussion of section II, we will approximate the

behavior of an exploding pusher, by assuming that it consists of 3 distinct, and to a large extent, uncoupled phases. These are, in order of temporal sequence.

1. The heating phase during which the pusher/fuel interface acelerates to a significant velocity.
2. The acceleration or useful energy phase.
3. The compression phase.

For pedagogical reasons, let us consider these processes in a slightly different order than they are listed.

THE COMPRESSION PHASE

Lasnex 1-D simulations suggest that for exploding pusher targets operating near their optimum performance, the average compressed fuel density can be approximated by, that produced by filling the initial target volume by the imploding fraction (1/2) of the pusher mass.[7] That is, the compression can be written as

$$C \sim \frac{3}{2} \frac{\rho_p}{\rho_o} \frac{w}{r_o}$$

where ρ_p and ρ_o are the pusher and initial DT fuel densities and w and r_o are the shell wall thickness and radius, respectively. Comparing this with Lasnex simulations, and α imaging experiments[18,19] suggest that

$$C_{(Lasnex)} \sim 3.5\ C, \quad \text{and} \quad C_{exp} \sim 2.3\ C.$$

This appears to be independent of the incident laser power and final neutron yield and thus has the interesting consequence that the final DT ion fuel temperature can be determined independently of the compression. This will be explored further during the discussion of the acceleration phase. For development of a simple model to predict experimental results, the assumption

will be made that the average fuel compression ratio is given by

$$C = 2.3 \times \frac{3}{2} \frac{\rho_p}{\rho_o} \frac{w}{r_o} = 8.63 \times 10^3 \frac{w}{\rho_o r_o} \qquad (1)$$

Here w and r_o are measured in μm and ρ_o in mg/cc.

THE EXPLOSION PHASE

This phase is characterized by rapid heat addition to the glass pusher caused by energy deposition both by superthermal electrons and by a nearly supersonically propagating thermal wave driven by laser absorption at the critical density region. The explosion phase is assumed to be over when the shockwave generated by the large pressure differential between the hot dense pusher and the fuel, has propagated through the pusher and thus initiated the large scale, rapidly accelerating motion of the pusher/fuel interface.

Associating the break through of the shockwave with the time when the pusher/fuel interface acquires a substantial velocity is reasonable. Until then, the only expansion of the pusher is due to the volume heating from the superthermal electron energy deposition which imparts no substantial fluid motion to the pusher. To arrive at an estimate for when the pusher explodes, we idealize this process, and thus solve

$$\int_{-\infty}^{t_e} V_s(t)\, dt = nw \qquad (2)$$

for t_e. Here V_s is the instantaneous shock velocity, w is the initial pusher thickness and n is a number of order 1 to account for the slow thermal expansion of the pusher during the explosion phase. Assuming the shock Mach number is of order 1, we can substitute the speed of sound in the pusher, for the shock speed. The pusher sound speed is equal to $(\gamma RT_{ion})^{1/2}$ with γ the usual ratio of specific heats and R the appropriate gas constant, (as we

note that the pusher temperature ahead of the shockwave is approximately 10 eV by the time of shockwave breaks through the pusher).

Since the electron ion equilibration times are short compared to our times scales, T_{ion} (pusher) = T_e (pusher). We now make the assumption that T_e (pusher) is some constant fraction β, of the electron temperature at the critical region. This "constant" is, in reality, clearly a function both of time and position in the pusher. The argument for ignoring its variation, is that for exploding pushers performing near their optimum conditions, the explosion phase is confined to the very early part of the Gaussian laser pulse, where the power is a more slowly varying function of time, than during the acceleration phase. Using the flux-limiting argument, we relate the electron temperature at the critical region to the absorbed intensity, by

$$\eta I(t) = (Fn_e v_e k T_e)_{\text{critical region}} \tag{3}$$

with η the absorption fraction, I the incident intensity and F the flux limiter. Combining (2) and (3) and substituting the pusher sound speed for $V_s(t)$ we can write the explosion condition as

$$\int_{-\infty}^{t_e} \left(\frac{np(t)}{4\pi r_0^2}\right)^{1/3} dt = 0.17 \frac{nwF^{1/3}}{\beta^{1/2}} \tag{4}$$

with P(t) the incident laser power in TW, t in picoseconds and r_0 and w in μm and β is the ratio between the T_e in the pusher and T_e at critical. Taking F $\sim$ 1/30 as suggested by Lasnex calculations for a one parameter fit for conduction inhibition, β = 1/5 and n = 4 equation (4) becomes

$$\int_{-\infty}^{t_e} \left(\frac{np(t)}{4\pi r_0^2}\right)^{1/3} = 0.49w \tag{5}$$

Solving this for the 0.45 TW, 50 psec, 70 μm diameter by 0.4 μm wall target mentioned in part II, produces a value for t_e of 45 psec before the peak of the pulse, and n = 4 is equivalent to assuming the pusher/fuel interface having moved 2 x w = 0.8 μm by $t = t_e$. These values are in good agreement with the data in figure 3, indicating that our choices for F, n, and β are reasonable.

The simple model prescription for determining the point on the Gaussian input pulse when the pusher explodes is thus given by equation (5) and the assumption that the pusher/fuel interface has moved in twice the original pusher wall thickness at that time.

THE ACCELERATION OR USEFUL ENERGY PHASE

During this phase the pusher/fuel interface is assumed to reach its peak velocity, at which time the implosion process is assumed to be effectively uncoupled from further absorption of the laser light. Referring to the specific 1-D simulation in Part II and figures 3 and 4, this condition was reached when the pusher/fuel interface had moved in ∿ 32% of the initial radius. Truncating the laser pulse at this time in the Lasnex calculation, produced 2/3 of the maximum neutron yield, with no significant change in the pusher/fuel interface trajectory. The final compression for that calculation, was 75, or equivalently, the pusher/fuel interface traversed 76% of the initial radius before stagnating. We note that for experimental modeling, the respective numbers would have been 50 and 73%. For the simple model, it will be assumed that these two ratios of 32% to 76% (0.42) and 32% to 73% (0.44) are canonical values determining the fraction of the absorbed energy which is "useful" for determining the neutron yield. Using the expression for the compression given by equation (1) and the results from the discussion of the explosion phase, we can then find the "cut-off" condition by solving

$$\int_{t_e}^{t_c} V_p(t)\, dt = 0.44\, r_o\left(1 - C_{exp}^{-1/3}\right) - 2w \qquad (6)$$

for t_c, with $V_p(t)$ the instantaneous pusher/fuel interface velocity. The useful absorbed energy, Ec, is thus defined as

$$E_c = f\eta \int_{-\infty}^{t_c} P(t)\, dt \qquad (7)$$

with f being that fraction of the absorbed energy which goes into the imploding fraction (assumed to be 1/2) of the pusher mass. The pertinent questions now are:

a) How to find $V_p(t)$
b) What is f.
c) Given E_c, how do we determine the fuel averaged DT ion temperature.

Let us tackle these questions in the inverse order of appearance.

a) Given that the assumption of that a cut-off condition has merit, i.e. that the laser pulse may be truncated at $t = t_c$ without significantly affecting the target performance and ignoring conduction losses during the compression phase for $t > t_c$, the most simple minded approach is to set

$$\alpha E_c = \left(\alpha \tfrac{3}{2} N_p k T_p + \tfrac{3}{2} N_i k T_i + \tfrac{3}{2} N_e k T_e\right)_{\text{Stagnation}} \qquad (8)$$

Here N_p, N_i, and N_e are the total number of pusher particles, fuel ions and fuel electrons, respectively, T_p, T_i and T_e are the pusher temperature, the fuel ion temperature and the fuel electron temperature respectively and α represents that fraction of the pusher mass which has stagnated at peak compression, and is in thermal equilibrium with the fuel. This statement is also consistent with the derivation of the average compression done earlier. Lasnex calculations suggest that $T_e \lesssim 1/5\ T_i$ at stagnation. Setting $T_p = T_i = T$, the fuel averaged DT burn temperature, assuming that $\alpha = 1/4$ and that the average charge state of the

pusher is 9, equation (8) is easily evaluated to give

$$T = 13.9 \frac{E_c}{M_p} \frac{1}{1+10^{-3} \frac{\rho_o r_o}{w}} \qquad (9)$$

With E_c in Joules, M_p = 1/2 of the pusher mass in nanograms, ρ_o the initial DT fuel density in mg/cc and r_o and w in μm.*

b) Measurements of the asymptotic ion expansion energy indicate that approximately 25% of the absorbed energy escapes in the form of fast ions which do not contribute to the implosion process. Simply dividing the remaining absorbed energy equally between the inward and outward moving portions of the pusher mass, results in f = 3/8.

c)Inspection of the Lasnex 1-D simulation mentioned earlier, suggest that for times greater than $t = t_e$,

$$(1/2)M_p V_p^2(t) = \frac{1}{8} \eta \int_{-\infty}^{t} P(t)\, dt \qquad (10)$$

With M_p being the inward moving portion of the pusher. Thus roughly 1/3 of the energy absorbed by M_p is assumed to go into kinetic energy.

To summarize the acceleration, or useful energy phase in the model; combining equations (6) and (10), we find t_c, the cut-off time by solving

$$\int_{t_e}^{t_c} \left[\frac{2\eta}{8M_p} \int_{-\infty}^{t} \left(P(x)\, dx\right)\right]^{1/2} dt = 0.44\, r_o \left[1 - \left(8.63 \times 10^{-3} \frac{w}{\rho_o r_o}\right)^{-1/3}\right] - 2w \qquad (11)$$

*The earlier version of the simple model had $T \sim E_c/M_p$ only, i.e. equivalent to ignoring N_f w.r.t. N_p in equation (8). Discussions with Damon Giovanelli of LASL, lead to the present form of equation (9) which also gives the model the ability to predict the neutron yield dependence on initial DT fill.

From equation (7) we define the useful fraction of the absorbed energy as

$$E_c = 3/8\ \eta \int_{-\infty}^{t_c} P(t)\ dt \qquad (12)$$

and once having found E_c, the fuel averaged DT ion temperature is found from equation (9).

A graphic representation of this three phase modeling of the exploding pusher behavior, and thus the prescription for finding E_c, is shown in figure 4 where we compare the pusher/fuel interface velocity and trajectory history as determined from solving equations (1) - (12) with the Lasnex 1-D simulation mentioned in Part II. The solid curve is the 1-D result when the Gaussian input pulse is truncated at the time when the shell has moved in 32% of the initial radius. The dashed lines show the result of applying the prescription outlined above. This model is thus equivalent to assuming that the shell "integrates" the absorbed energy until the shockwave has propagated through the pusher and completed the explosion phase at time $t = t_e$ as found from equation (5). At this point the pusher/fuel interface is assumed to have moved in a distance of 2 w and acquired an initial velocity proportional to the square root of the absorbed energy until that time. It then continues with velocity proportional to the square root of the absorbed energy at any given time, until $t = t_c$. The assumption is then made that at this time the inward moving pusher and fuel are uncoupled from further absorption of laser energy, and continues with constant velocity until the final radius as determined from equation (1). Comparison of equations (9), (10), and (12) shows that for fixed target parameters, $T \sim E_c/M_p \sim V_p^2(t = t_c)$, i.e. the final fuel averaged DT ion temperature is proportional to the square of the peak pusher velocity obtained. This is in good agreement with Lasnex 1-D simulations and also ties in with the earlier observation that the initial strong shockwave and the succession of spherically imploding weaker shockwaves generated by the pusher as it is accelerated to it's peak velocity are significant in determining the final DT burn temperature.

NEUTRON PRODUCTION

Neglecting fuel depletion, the number of thermonuclear neutrons produced by a DT plasma is assumed to be given by

$$N = \int dt \int d^3r \; n_D n_T \; \langle \sigma v \rangle$$

In general, this integral must be carried out over all time and space where n_D and n_T are deuterium and tritium number densities and $\langle \sigma v \rangle$ is the Maxwell averaged DT cross section. While not strictly correct, an estimate for the neutron yield of an inertially confined plasma may be made by assuming that the ions are isothermal at an ion temperature T and isotropic in a volume V for the duration of the inertial confinement burn time $\Delta\tau$. Consequently,

$$N \simeq n_D n_T \; \langle \sigma v \rangle \; V \; \Delta\tau \qquad (13)$$

The fuel densities and volume prior to the laser driven implosion are related to these parameters during the burn by the burn averaged volume compression C For an equimolar mixture of DT

$$n_D = N_T = 1.2 \times 10^{20} \; \rho_o \; C$$

with ρ_o the initial DT density in mg/cc. Similarly,

$$V = 4/3\pi r_o^3/C$$

where r_o is the initial uncompressed fuel radius. An estimate for the burn time, $\Delta\tau$, arises from the assumption that the confinement-reaction time is proportional to the time required for a rarefaction wave to traverse the fuel; i.e., $\Delta\tau$ is proportional to the compressed radius divided by the ion sound speed. Detailed Lasnex 2-D simulations suggest that the proportionality constant is $1/\frac{1}{4}$, thus

$$\Delta\tau = \frac{1}{1/\frac{1}{4}} \frac{r_o/C^{1/3}}{\sqrt{\frac{5}{3}\frac{k}{m}T_{ion}}}$$

The Maxwell averaged DT reaction cross section is accurately approximated[33] by

$$\langle\sigma v\rangle = 3.8 \times 10^{-12}\, T^{-2/3} \exp(-19.02/T^{1/3})$$

Replacing C by $8.63 \times 10^3 \frac{w}{\rho_o r_o}$ from equation (1) and inserting these relationships into equation (13) yields

$$N = 2.73 \times 10^8\, \rho_o^{4/3}\, r_o^{10/3}\, w^{2/3}\, T^{-7/6} \exp(-19.02/T^{1/3}) \qquad (14)$$

with ρ_o the initial DT fill in mg/cc, r_o and w the initial radius and pusher thickness in μm and T, the fuel averaged DT ion temperature, in keV.

Summarizing the 3 phases, we obtain T from

$$T = 13.9 \frac{E_c}{M_p} \frac{1}{1 + 10^{-3}\frac{\rho_o r_o}{w}}, \qquad M_p = \frac{1}{2}\text{ Pusher Mass},$$

with

$$E_c = 3/8\,\eta \int_{-\infty}^{t_c} P(t)\,dt$$

where t_c is found by solving

$$\int_{-t_e}^{t_c} \left(\frac{2\eta}{8M_p} \int_{-\infty}^{t} P(x)dx \right)^{1/2} dt = 0.44 r_o \left(1 - \left(8.63 \times 10^{-3} \frac{w}{\rho_o r_o} \right)^{-1/3} \right) - 2w$$

and t_e is found from

$$\int_{-\infty}^{t_e} \left(\frac{\eta\, P(t)}{4\pi r_o^2} \right)^{1/3} dt = 0.49\, w$$

For a Gaussian temporal input laser pulse with a FWHM of τ (psec), the following prescription provides a convenient method for obtaining the performance of an individual exploding pusher target experiment.

(1) Define

$$F(z) = \int_{-\infty}^{Z} \frac{1}{\sqrt{2\pi}} e^{-u^2/2}\, du$$

i.e. the normal probability function tabulated in standard mathematical tables.

(2) Find the explosion time by solving

$$F(z_e) = 0.6\, \frac{w}{\tau} \left(\frac{r_o^2}{P_o\, \eta} \right)^{1/3} \quad ; z_e = 1.36\, \frac{t_e}{\tau}$$

(3) Find the compression by

$$C = 2.3 \times 3/2 \frac{2.5}{\rho_o \times 10^{-3}} \frac{w}{r_o}$$

(4) Find the cut off time by solving

$$\int_{x_e}^{x_c} \sqrt{F(x)}\, dx = 0.572 \frac{\Delta r_o}{\tau} \sqrt{\frac{r_o^2 w}{\eta P_o \tau}}$$

with $x_e = 2.35 \frac{t_e}{\tau}$, $x_c = 2.35 \frac{t_c}{\tau}$ and

$$\Delta r_o = 0.44\, r_o (1 - C^{-1/3}) - 2w$$

(5) find

$$E_c = \frac{3}{8} \eta P_o \tau F(x_c); \qquad x_c = 2.35 \frac{t_c}{\tau}$$

(6) Find

$$M_p = 1.57 \times 10^{-2} r_o^2 w$$

(7) Find

$$T = 13.9 \frac{E_c}{M_p} \frac{1}{1 + 10^{-3} \frac{\rho_o r_o}{w}}$$

(8) Find

$$N = 2.73 \times 10^8 \rho_o^{4/3} r_o^{10/3} w^{2/3} T^{-7/6} \exp(-19.02/T^{1/3})$$

Where

ρ_0	is initial DT fill in mg/cc
r_0, w, Δr_0	are in μm
τ,t	are in psec ($\tau$is laser FWHM)
P_0	is the peak power in TW
η	is the absorption fraction
T	is the model derived fuel averaged DT ion temperature in keV.

The simple model, however, should not in principle be limited to Gaussian temporal laser pulses. As long as the early energy rise is rapid enough, and the laser intensity and target parameters are such that the target operates in the exploding pusher mode, the model should work equally well. However, now equations (5)-(12) must be used in their original form. This will also be discussed in the next section in conjunction with comparing the model predictions to experimental results obtained with the LASL CO_2 laser whose pulse shape has been approximated by a triangular temporal distribution.

IV COMPARISON OF THE SIMPLE MODEL TO EXPERIMENTS RESULTS AND LASNEX SIMULATIONS

As mentioned in the introduction, the neutron yield is one of the more sensitive indications of the success of any implosion fusion.

experiments. Plotted against an improper parameter, however, trends and proper scaling relations will not be apparent. This is shown in figure 8 where the neutron yield from a variety of experimental conditions are plotted as a function of peak input power. The open data points are from the LLL Janus, Cyclops and Argus 1.06 μm Nd:glass laser facilities utilizing f/1[10,12, 15] f/2.5[13] and lens/elliptical-mirror[14] focusing optics with Gaussian temporal pulses. The solid points are recent results from LASL using their 10.6 μm CO_2 laser having triangular temperal pulse with a (10-90%) rise time of ∿ 160 psec and a fall time of ∿ 2.2 nsec.[34] The absence of any relevant trend or scaling parameter is obvious. Taking the optimum results, the peak neutron yield appears to be increasing approximately as the peak power squared. This however, would clearly not inform an experimenter of which direction to change his target and laser parameters from a nonoptimal result. In comparison, figure 9 shows the same data normalized by $\rho_0^{4/3} r_0^{10/3} w^{2/3}$ as suggested by equation (14) and plotted versus the model inferred fuel averaged DT ion temperature from equation (9). The correlation has clearly improved, collapsing nearly all the data to the model predicted curve. The veritical error bars indicate experimental uncertainty in the neutron yield, while the horizontal error bars indicate the uncertainty in the absorbed energy, which ranged from ∿ (13 ± 4)% for the f/2.5 Cyclops results up to a maximum of (45 ± 5)% for the Hyperion results on Argus that yielded 1.6×10^9 neutrons. Considering that the experimental parameters ranged from P_0 ∿ (0.2 - 4.4)TW, w ∿ (0.4 - 1.2) μm, r_0 ∿ (20-100) μm and ρ_0 ∿ (0.16 - 9) mg/cc the agreement is indeed satisfactory. The model inferred DT ion temperatures are also in reasonable agreement with those inferred from alpha and nuetron time-of-flight measurements, as indicated in Table I.

Figure 10 shows the variation of neutron yield with initial DT fill for experiments performed on the Janus laser. The experimental conditions are listed in the figure and the solid curves are the ranges of the model predictions within the measured absorption values. Both the general magnitude

of the yields and the shape of the curves are in good agreement. Figure 11 shows the variation of neutron yield with initial target diameter. Here the neutron yield is normalized as indicated to remove the density, wall thickness and laser condition variations, as the data again spans more than a decade in incident peak power and nearly a factor of 7 in laser pulse FWHM. The least squares fit through the data giving a slope of 3.28 is in good agreement with the expected slope of 10/3. Finally, figure 12 shows an example of specific experimental results compared with the model predictions. The experimental parameters are listed on the figure, and were chosen to represnet a cross section of the experimental parameter space with neutron yields from $\sim 10^3$ to $\sim 10^9$. The agreement is reasonable, and together with figures 9-11 lend considerable after-the-fact credence to the simplifying assumptions that were made during the development of the model. It not only suggests that not too much of the physics was "swept under the rug," but that the picture of an exploding pusher that is defined within the limitations of the assumptions is a reasonable one.

Figures 13-16 compares the model with 1-D Lasnex simulations. As was mentioned in Part II, the average compressions seen in the 1-D simulations were higher than those seen in experiments, in addition, the 1-D simulations generated higher DT ion temperatures than those observed. To compensate for this, equation (1) was replaced by

$$C = 3.5 \times 3/2 \frac{\rho_p}{\rho_o \times 10^{-3}} \frac{w}{r_o}$$

and equation (2) was replaced by

$$T = 18.5 \frac{E_c}{M_p} \frac{1}{1 + 10^{-3} \frac{\rho_o r_o}{w}}$$

However, even with these substitutions, it was found necessary to multiply the computed neutron yield by 5 in order to reproduce to neutron yield for the

simulation mentioned in Part II which served as a baseline for the model development. The factor of 5 may in part be accounted for by the increased symmetry of compression in the 1-D simulation over the actual experiments. This is also borne out by the fact that the experiments using the spherical illumination system in a geometry to produce implosions more nearly simulating the 1-D spherical geometry, resulted in a neutron yield that was on the average 2.5 times greater than that produced with f/1 lenses under similar conditions.

Figure 13 shows the neutron yield for several different wall thicknesses irradiated with laser powers and pulse widths varying from 0.5 to 20 TW and 30-200 psec, plotted as a function of initial target diameter. The agreement to within a fraction of 2 over 6 decades in neutron yield is gratifying. Figure 14 shows the neutron yield for a variety of target parameters and laser input power, plotted as a function of the laser pulse FWHM. Again the agreement is reasonable. The divergence at shorter pulse lengths, as well as the divergence in figure 13 for increasing initial diameter, is related to a deviation from proper matching of the FWHM to the implosion time scale, and will be discussed in Part V. Figure 15 shows comparison between 1-D simulations and the simple model for optimum exploding pusher designs. For simulations with similar absorption fraction, the approximate squared dependence on input power mentioned earlier for optimum designs is evident. Figure 16 shows a comparison between the model and 1-D simulations[35] for a totally different regime of the exploding pusher parameter space. A thick-walled, small diameter target irradiated with a long pulse, was used in the simulation to obtain average compressions approaching 1000. Again the agreement between the model and the 1-D simulation is reasonable. The deviation as the input power goes to zero is expected. As the incident power decreases, keeping other parameters fixed, we move more and more towards an ablative mode, and would thus expect the model and the simulations to deviate, and the model to predict a higher neutron yield since it still assumes that 1/2 of the mass explodes inward and obtains 1/2 of the absorbed energy.

V. LIMITATIONS OF THE SIMPLE MODEL

Some of the limitations of the model have already been discussed in the previous sections. The major regimes where the model fails and a brief discussion of the most plausible reasons are summarized below.

1) The "Ablative" Regime

This is characterized by the deviation between 1-D simulation and the model seen in Fig. 16 as the input power decreases. As the power, and hence the incident energy, decreases, the time required to "explode" the pusher increases in the model, to the point that for 0.1 TW, $\sim$ 20% of the available energy is required to "explode" the pusher. Not only is this considerably further up on the Gaussian pulse than was assumed to derive the model, but the decreasing incident intensity with the concommitant softer superthermal electron spectrum, coupled with the thick wall, means that the target is approaching an ablative mode of operation. It is not a question of poor mismatch between the implosion time and pulse FWHM. For the 0.1 TW case, for example, stagnation is reached for $t/\tau \sim 0.8$ after the peak of the pulse which compares favorably with figure 3 and only 40% of the available absorbed energy was used to reach t_c. The model was an attempt to mock up the situation where the pusher not only explodes, but there is significant preheat of the fuel prior to the compressive heating following $t = t_c$. For the conditions on figure 16, the thick wall and lower intensity result in a reduced explosive nature of the pusher acceleration and reduced preheat, neither of which is included in the model. An appropriate criterion for defining this regime, is that the pusher thickness w should not be much greater than the superthermal electron mean free path[7] and that $t_e/\tau < -0.3$ before the peak of the pulse ($t/\tau = 0$).

2) The Massive Target Regime

This is characterized by the divergence observed in figure 13 as the diameter increases significantly beyond the optimum value, and in figure 14 as the pulse length becomes too short. In contrast to the previous case, here we see the effect of a significant mismatch between the laser FWHM and the

implosion time scale. As the FWHM decreases or the diameter increases, for otherwise fixed target and laser conditions, a point is reached when there simply is not sufficient energy available. This is shown in more detail in Figure 17a and 17b. For D > 200 μm in figure 17b, for example, all the available absorbed energy (> 99.8%) is needed for the pusher to get to $t = t_c$, and the stagnation would occur at $t/\tau \sim 5.5$ after the peak of the pulse. For the optimum point, however, the corresponding numbers are 75% and $(t/\tau)_{stagnation} \sim 2$, which are more in line with data from figure 2 and part II. A similar set of numbers apply to the situation where the pulse length is decreased, keeping laser power and target parameters fixed. In addition, as the time required to reach stagnation increases significantly with respect to the laser pulse FWHM, the time scales for conduction losses during the compression phase can no longer be ignored. An appropriate criterion for defining this regime would then be that the model can no longer be expected to apply if the energy required to reach $t = t_c$ exceeds 90-95% of the total available energy absorbed by the pusher.

3) The Superthermal Electron Runaway Regime

This is characterized by a mismatch in the pusher thickness and the superthermal electron mean free path in the other direction of that discussed above, i.e., of the form $w << \lambda_e$, an example of which is shown in figure 18. As the incident laser intensity increases, both the fraction of the absorbed energy which appears in the superthermal electron distribution and their effective temperature, Θ_{hot}, increases. If the pusher thickness is not increased to compensate for this, the result is a lower coupling efficiency between these electrons and the pusher and an increase in the production of radially directed very high energy pusher ions. For sufficiently high intensities and thin pusher walls, a situation can arise where effectively all the absorbed energy is used to convert essentially the entire pusher mass to a high energy, outward directed ion expansion. For this situation there is simply not enough inward moving pusher mass to do efficient work on the fuel, and the model would clearly over estimate the yield. Detailed Lasnex calculations indicate that such a situation will arise for intensities in excess of $\sim 10^{17}$ W/cm^2 and $w \lesssim 0.5$ μm targets. There is, however, no unique set of conditions above

which electron run-away occurs. A factor such as the rate of power increase is clearly also important, i.e. an intensity and wall thickness that produces the "runaway" effect, as say 50 psec, may not do so at 200 psec.

VI CONCLUSION

A simple model has been developed which can be used to scale neutron yields for variations in initial DT fill, wall thickness, target radius, and laser input conditions. The model also illucidates the more important processes occuring in exploding pusher experiments. Agreement to within a factor of two over 6 orders of magnitude in neutron yield for a large portion of the target and laser input parameter space has been obtained both for experimental results and Lasnex 1-D simulations.

TABLE I

Comparison of model derived fuel average DT ion temperatures with neutron and alpha time-of-flight data.

Shot ID	Fuel Averaged T_{ion} From n and α Time-of-flight	Fuel Averaged T_{ion} From Model
36120910	5.2	5.0
36120702	5.5	4.3
36120911	6.5	8.0
36120906	6.8	6.7
36100116	7.5	6.4
36100115	7.9	6.8

REFERENCES

1. J. H. Nuckolls, LLL UCRL-76395 (1975).
2. G. H. Dahlbacka and J. H. Nuckolls, LLL UCRL 75885 (1974).
3. Y. B. Zeldovich and Y. P. Raizer, "Physics of Shock Waves and High Temperautre Hydrodynamic Phenomena", Academic Press, Vol. II p. 552 (1966).
4. J. T. Larsen, LLL UCRL-77040 (1975).
5. J. T. Larsen, LLL UCRL-77901 (1976).
6. J. T. Larsen, LLL 1976 Laser Program Annual Report, UCRL 50021-76, Section T-306 and T-422.
7. J. H. Nuckolls, LLL 1976 Laser Program Annual Report, UCRL-50021-76, Section T-305
8. J. H. Nuckolls, L. Wood, R. Thiessen and G. Zimmerman, Nature 239, 139 (1972)
9. G. B. Zimmerman, LLL UCRL-74811 (1973).
10. E. K. Storm, et. al., LLL 1975 Laser Program Annual Report, UCRL 50021-75, Section 8
11. J. F. Holzrichter, et. al., Plasma Physics, 18, 675 (1976)
12. E. K. Storm, LLL 1976 Laser Program Annual Report, UCRL-50021-76, Sections T-421 and T-423.
13. K. R. Manes, LLL 1976 Laser Program Annual Report, UCRL-50021-76, Sections T-401, T402, and T-407.
14. E. K. Storm, et. al., To be published in APL, Manuscript #3280R.
15. E. K. Storm, et. al., To be published in Phys. Rev. Lett., Manuscript #LB1116.
16. D. T. Attwood, et. al., Phys. Rev. Lett., 37, 499 (1976).
17. D. T. Attwood, et. al., Phys. Rev Lett., 38, 282, (1977).
18. N. M. Ceglio and L. W. Coleman, Phys. Rev. Lett., 39, 20 (1977).
19. V. W. Slivinsky, et. al., A.P.L., 30, 11, p. 555 (1977).
20. V. W. Slivinsky, et. al., to be published in J.A.P.
21. V. C. Rupert, et. al., J.A.P. (in press).
22. D. W. Phillion et. al., LLL UCRL-79769 (1977).

23. K. R. Manes, V. C. Rupert, J. M. Auerbach, P. Y. Lee, and J. E. Swain, Phys. Rev. Lett., 39, p. 5 (1977).
24. D. W. Phillion, et. al., Phys. Fluids (to appear in November, 1977)
25. D. T. Attwood, et. al., LLL UCRL-79794 (1977).
26. W. Kruer, R. Haas, W. Mead, D. Phillion, and V. Rupert, in Plasma Physics: Non-linear Theory and experiments, p. 64-81, edited by H. Wilhelmsson (Plenum, New York, 1977.
27. K. G. Estabrook, E. J. Valeo and w. L. Kruer, Phys. Fluids, 18, p. 1151 (1975).
28. Y. B. Zedovich and Y. P. Raizer, "Physics of Shock Waves and High Temperature Hydrodynamic Phenomena," Academic Press, Vol. I, p. 421 (1976)
29. R. E. Marshak, Phys. Fluids, 1, 1, p. 24 (1958).
30. J. E. Swain, H. G. Ahlstrom, A. Glass, K. R. Manes, E. K. Storm, F. Rienecker, J. A. Monjes, D. E. Campbell, and L. Seppala, UCRL-78445 (1976).
31. C. E. Thomas, Appl. Opt., 14, 1257 (1975).
32. G. Charatis, J. Downard, R. Goforth, B. Guscott, T. Henderson, S. Hildum, R. Johnson, K. Moncur, T. Leonard, F. Mayer, S. Segall, L. Siebert, D. Solomon, and C. Thomas, Proceeding 5th IAEA Plasma Fusion Conference, Tokyo, Japan (1974).
33. K. A. Brueckner and S. Jorna, Rev. of Mod. Phys. 46, 2, p. 325 (1974)
34. D. Giovanelli, LASL, Private Communication (September, 1977).
35. Y. L. Pan, LLL, Private Communication (April, 1977).

FIGURE CAPTIONS

Figure 1. A typical high power, high yield exploding pusher target experiment.

Figure 2. Continuum, space and time integrated x-ray spectra for exploding pusher targets at 0.4 and 4 TW. Both experiments were done using f/1 lenses irradiating $\sim$ 85 μm diameter, 0.8 μm thick DT filled S_iO_2 microshells.

Figure 3. 1-D Lasnex calculations of the pusher/fuel interface position and velocity as a function of time for a 0.45 TW, 50 psec (FWHM), 1.06 μm thick S_iO_2 microshell filled with 2 mg/cc of DT. The Gaussian input laser pulse is shown for time reference. The times t_1 - t_4 indicate times when the laser pulse was truncated in the calculation, to explore the concept of useful absorbed energy. The subscripts on the neutron yield N, the interface velocity V and position r, are the corresponding results. The implication is that truncating the input pulse after the pusher/fuel interface has moved in $\sim$ 32% of the initial radius does not significantly affect the target performance.

Figure 4. This shows the ratio of the neutron yield obtained by truncating the laser pulse in figure 3 at any given time, to the maximum neutron yield obtained. In addition it shows the pusher fuel interface as a function of time. The "knee" on the curve where $N/N_{max} = 2/3$ occurs when the interface has moved in $\sim$ 32%, and is chosen for the cut-off point in the simple model.

Figure 5. This shows a comparison between a Lasnex 1-D simulation and experimental results obtained on Janus using the spherical illumination system and the x-ray pinhole/streak camera.

Figure 6. This shows a comparison between Lasnex 1-D simulation and a one sided irradiation experiment. The experimental pusher/fuel interface velocity was assumed to be equal to the velocity of the maximum x-ray emission region as determined from the x-ray pinhole/streak camera data. The Lasnex simulation was for a two sided irradiation and thus can not be compared with experimental results past the calculated stagnation region.

Figure 7. This shows the model prescription for determining the pusher/fuel interface velocity and position history, and compares it with the Lasnex 1-D simulation used to derive at the model.

Figure 8. Neutron yield as a function of peak input power for expermiments using 1.06 μm Nd:glass lasers with $\sim$ f/0.07, f/1 and f/2.5 optics and 10.6 μm CO_2 lasers using f/2 optics.

Figure 9. This shows the data from figure 8 plotted as a function of the model derived fuel averaged DT ion temperature. The neutron yield is also normalized with $\rho_o^{4/3} r_o^{10/3} w^{2/3}$ as suggested by the model equations.

Figure 10. The neutron yield as a function of initial DT fill for f/1 irradiation experiments on the Janus laser at 0.39 TW. The model predicted yield was calculated using the average experimental parameters, and computing the yield for the upper and lower estimates of the absorption fraction. The neutron yield was also normalized by $r_o^{10/3} w^{2/3}$ to remove the target geometry dependence.

Figure 11. Normalized neutron yield plotted as a function of initial target diameter. The least squares fit gives a slope of 3.28, in reasonable agreement with the model predicted value of 10/3.

Figure 12. Experimental and model predicted neutron yield for a large range of experimental parameters.

Figure 13. Comparison of Lasnex 1-D simulations and model predicted yield variation with initial target diameter.

Figure 14. Comparison of Lasnex 1-D simulations and model predicted yield variation with laser pulse length (FWHM).

Figure 15. Optimum target design predictions form Lasnex 1-D and the simple model. For identical absorption parameter, the neutron yield scales approximately as the peak power squared.

Figure 16. Neutron yield and compressed DT density for thick walled, long pulse, low power exploding pusher targets. As the incident power approaches zero, the target behavior approaches the ablative mode, and the model is expected to over-estimate the yield.

Figure 17. The model starts to fail as the target becomes too massive for the available energy, causing a significant mismatch between the laser pulse length and the target implosion time scale. This is demonstrated for a 0.5 TW, 100 psec, 0.4 μm wall target in Fig. 17a, and a 2 TW, 65 psec., 0.7 μm wall target in Fig. 17b.

Figure 18. For high intensity and thin-walled targets, the superthermal electron mean free path is not well matched to the pusher, and causes a poor energy coupling efficiency. As the pusher thickness increases, the model predicts the correct yield.

TARGET AND LASER PARAMATERS

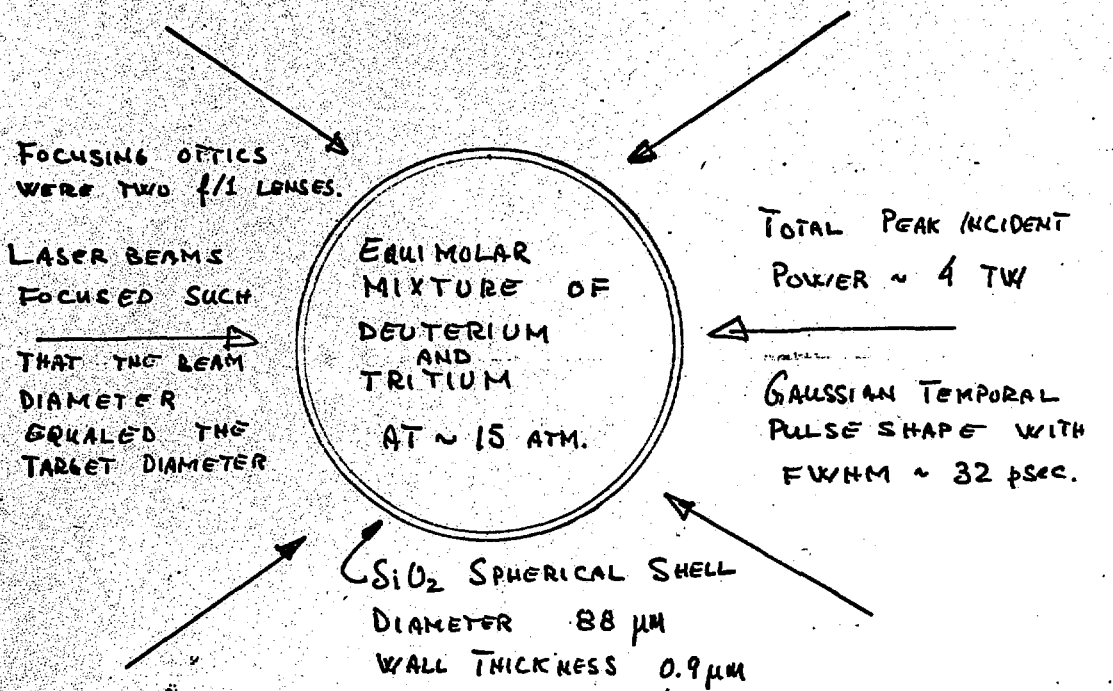

EXPERIMENTAL RESULTS

ENERGY ABSORBED	(22 ± 3) %
THERMONUCLEAR YIELD	$\bar{\alpha} = (7.9 \pm 1.4) \times 10^8$
	$\bar{n} = (8.0 \pm 1.5) \times 10^8$
FUEL AVERAGED ION TEMPERATURE (FROM α TOF)	(5.2 ± 1.5) keV
TIME AVERAGED COMPRESSION (FROM α IMAGE)	~54

FIGURE 1

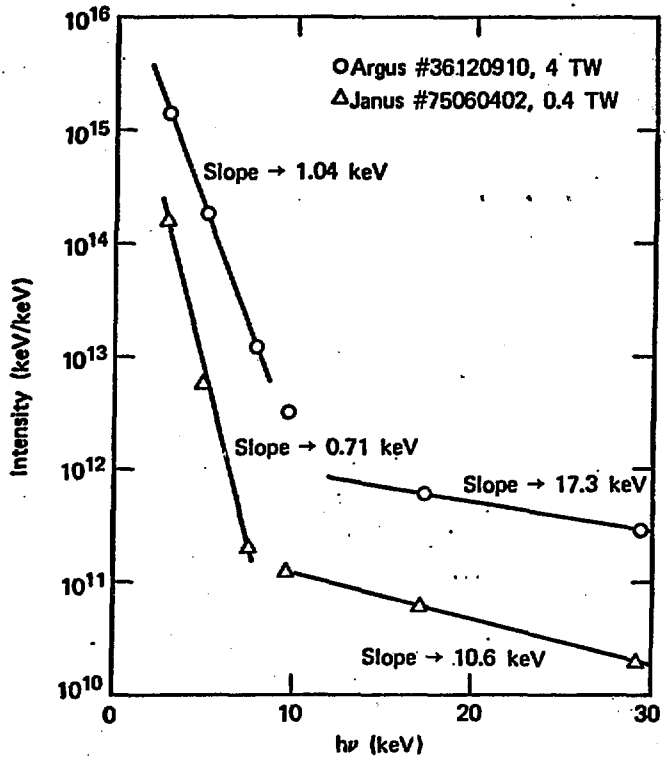
OArgus #36120910, 4 TW
ΔJanus #75060402, 0.4 TW
Slope → 1.04 keV
Slope → 0.71 keV
Slope → 17.3 keV
Slope → 10.6 keV
Intensity (keV/keV)
hν (keV)
10^16
10^15
10^14
10^13
10^12
10^11
10^10
0
10
20
30

FIGURE 2

LASNEX 1-D TARGET PERFORMANCE

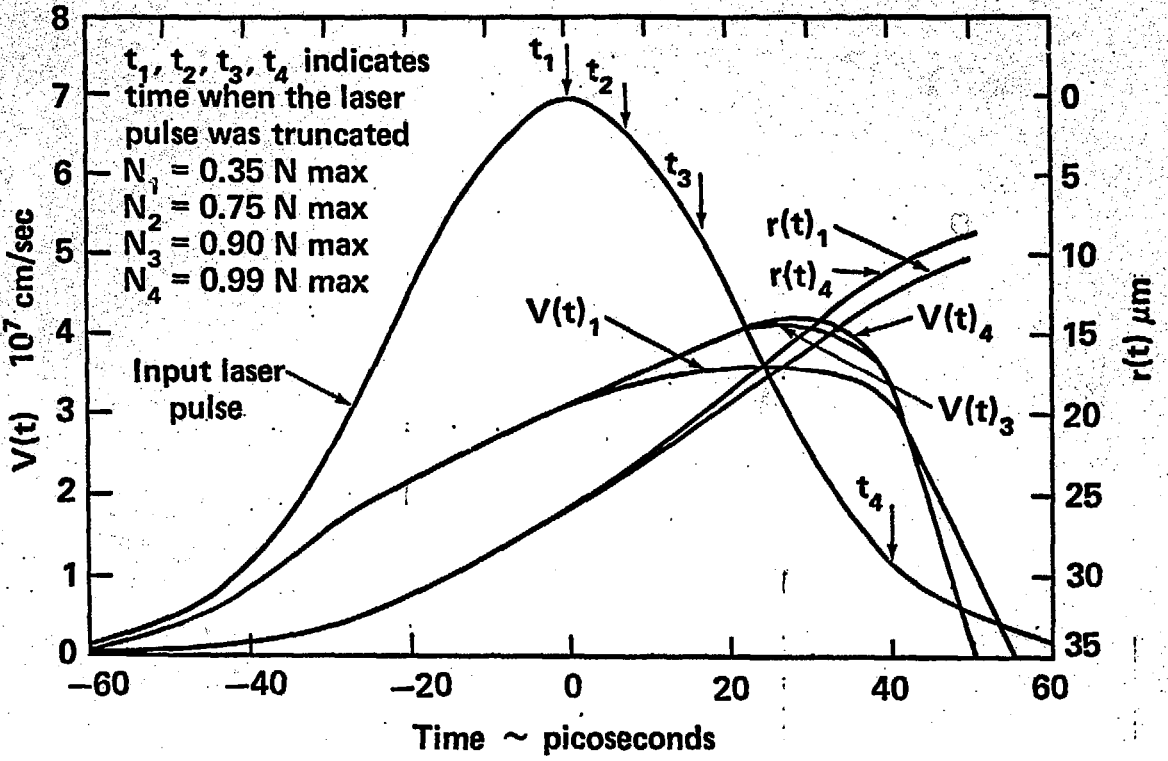

Figure 3

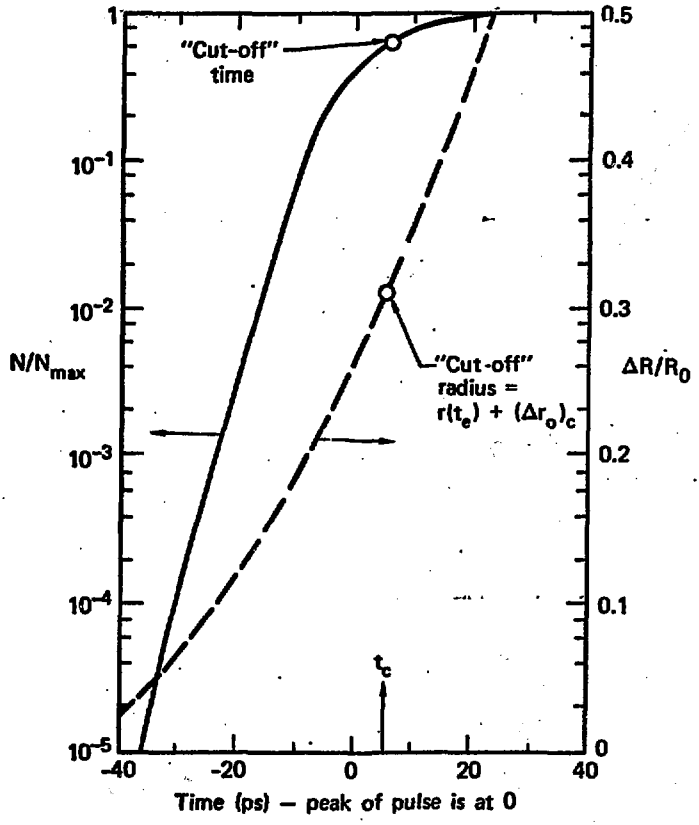
"Cut-off" time
"Cut-off" radius = $r(t_e) + (\Delta r_o)_c$
N/N_{max}
$\Delta R/R_0$
t_c
1
10^{-1}
10^{-2}
10^{-3}
10^{-4}
10^{-5}
0.5
0.4
0.3
0.2
0.1
0
-40
-20
0
20
40
Time (ps) — peak of pulse is at 0

FIGURE 4

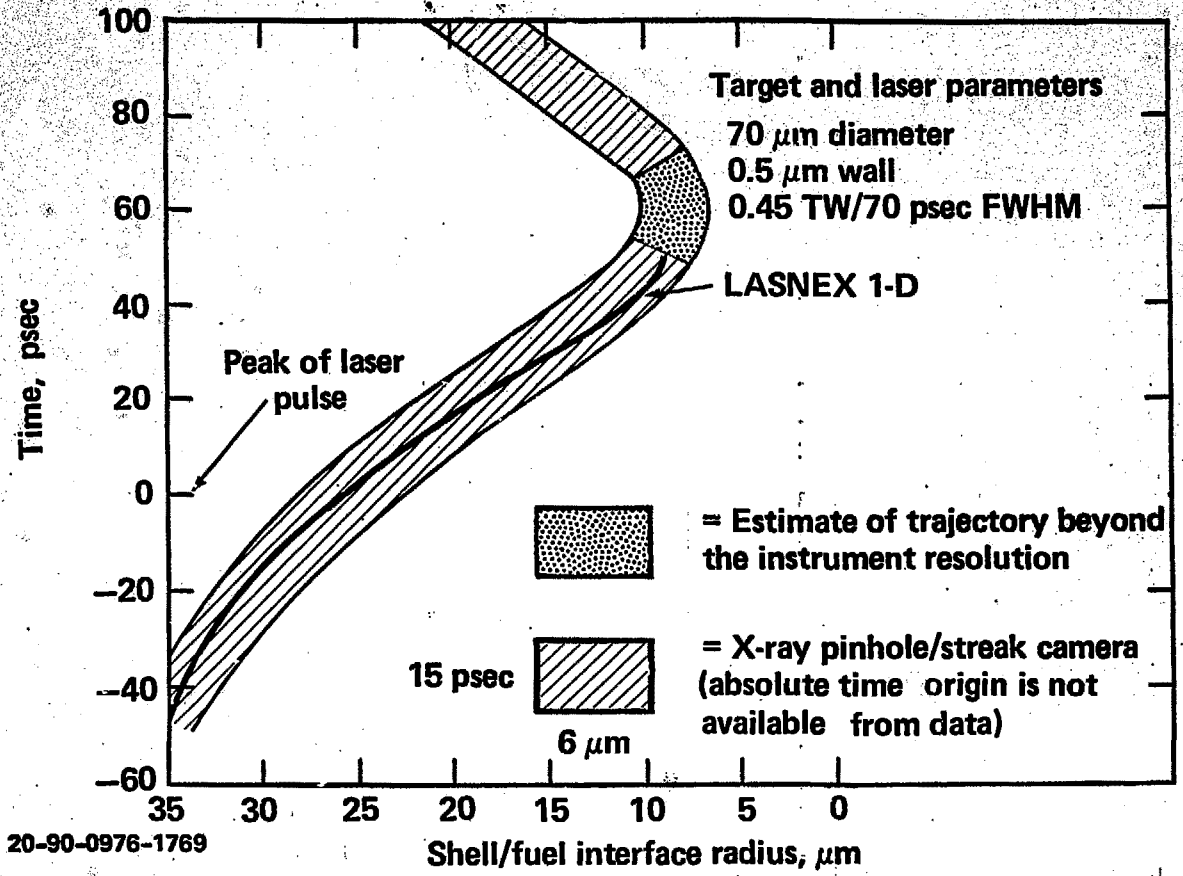
Target and laser parameters
70 μm diameter
0.5 μm wall
0.45 TW/70 psec FWHM
LASNEX 1-D
Peak of laser pulse
= Estimate of trajectory beyond the instrument resolution
= X-ray pinhole/streak camera (absolute time origin is not available from data)
15 psec
6 μm
Time, psec
100
80
60
40
20
0
−20
−40
−60
35
30
25
20
15
10
5
0
Shell/fuel interface radius, μm
20-90-0976-1769

Figure 5

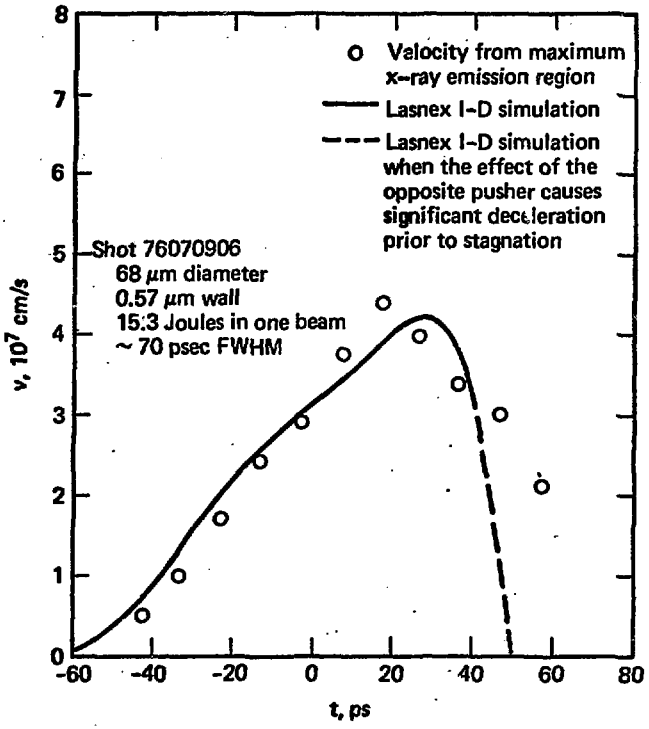
Velocity from maximum x-ray emission region
Lasnex I-D simulation
Lasnex I-D simulation when the effect of the opposite pusher causes significant deceleration prior to stagnation
Shot 76070906
68 μm diameter
0.57 μm wall
15.3 Joules in one beam
~ 70 psec FWHM
v, 10^7 cm/s
t, ps
0
1
2
3
4
5
6
7
8
-60
-40
-20
0
20
40
60
80

FIGURE 6

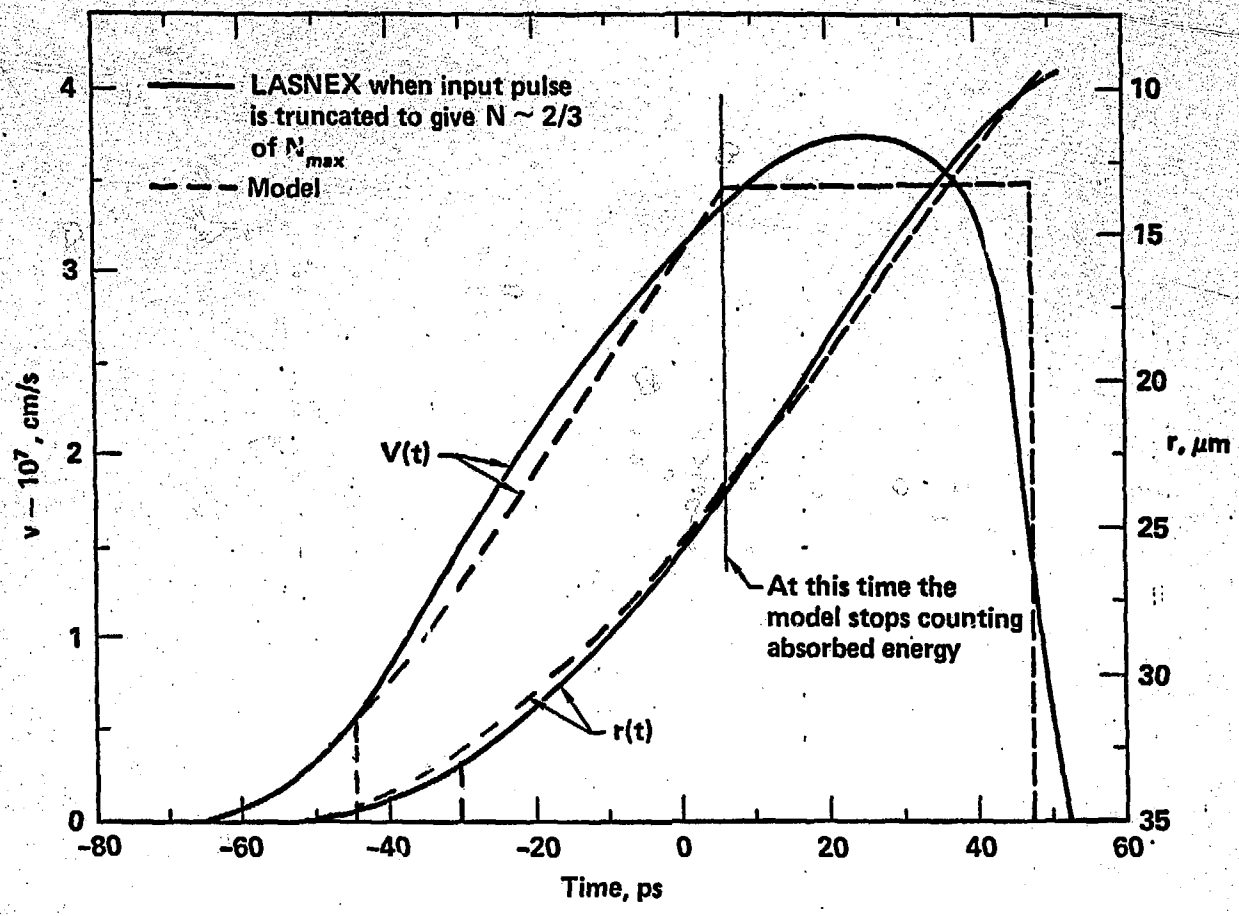
LASNEX when input pulse is truncated to give N ~ 2/3 of N_{max}
Model
V(t)
r(t)
At this time the model stops counting absorbed energy
v — 10^7, cm/s
r, μm
Time, ps
4
3
2
1
0
10
15
20
25
30
35
-80
-60
-40
-20
0
20
40
60

Figure 7

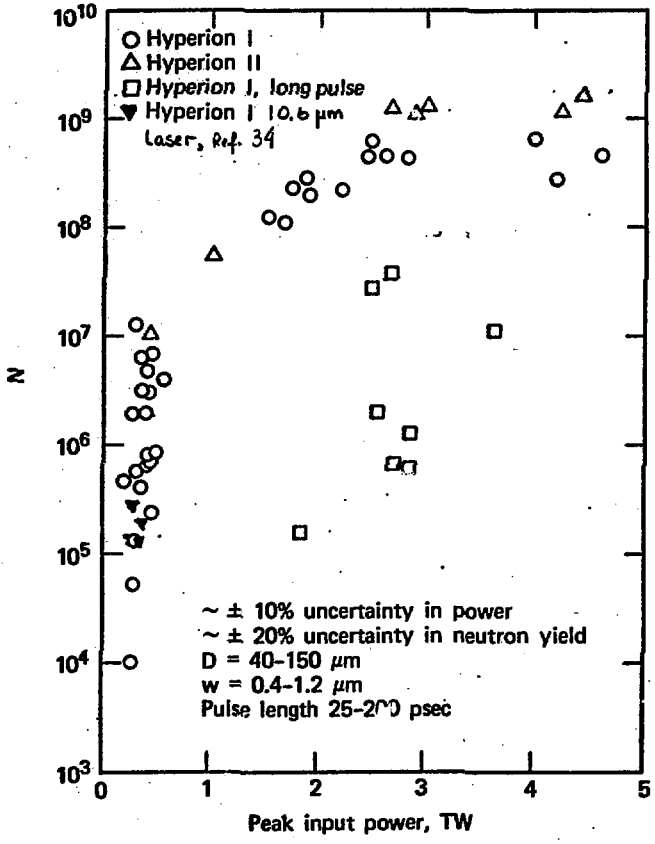
Hyperion I
Hyperion II
Hyperion I, long pulse
Hyperion I 10.6 μm
Laser, Ref. 34
~ ± 10% uncertainty in power
~ ± 20% uncertainty in neutron yield
D = 40–150 μm
w = 0.4–1.2 μm
Pulse length 25–200 psec
N
Peak input power, TW

FIGURE 8

NORMALIZED NEUTRON YIELD IS ADEQUATELY FIT BY THE SIMPLE MODEL

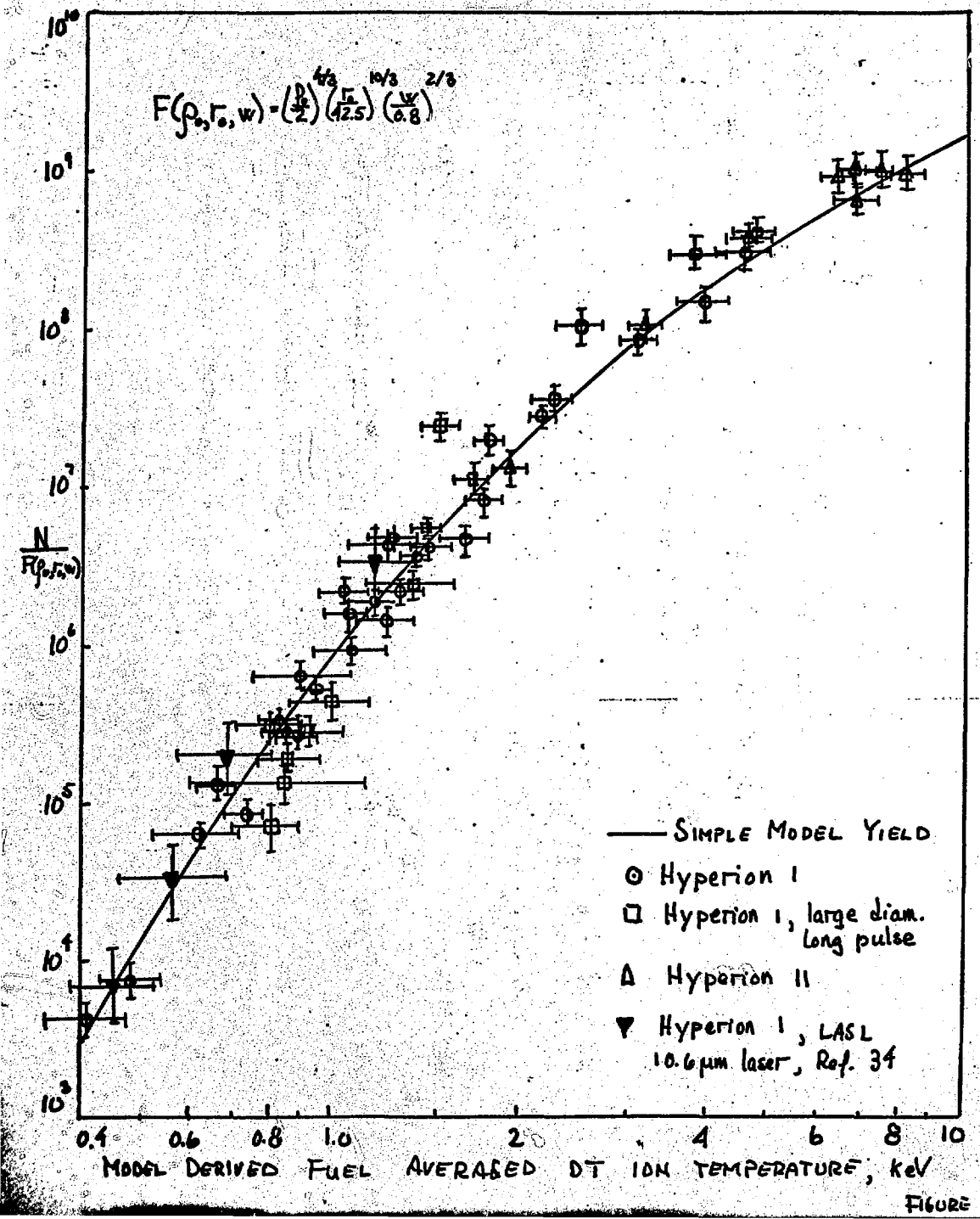

FIGURE 9

NEUTRON YIELD AS A FUNCTION OF DT FILL

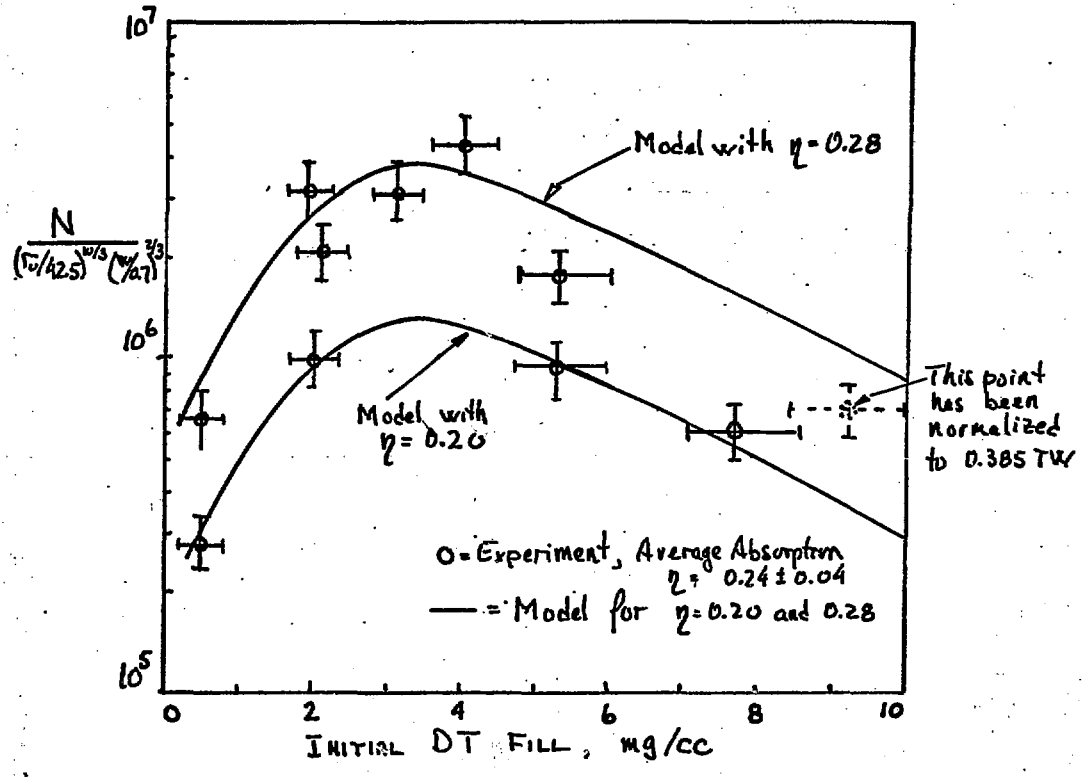

MODEL CALCULATIONS WERE PERFORMED FOR THE AVERAGE EXPERIMENTAL CONDITIONS

$P_0 = (0.385 \pm 0.025)$ TW
$\bar{\tau} = (75 \pm 6)$ psec
$r_0 = (42.5 \pm 0.5)$ μm
$w = (0.7 \pm 0.1)$ μm

FIGURE 10

NORMALIZED NEUTRON YIELD VS. TARGET DIAMETER
SIMPLE MODEL GIVES REASONABLE FIT

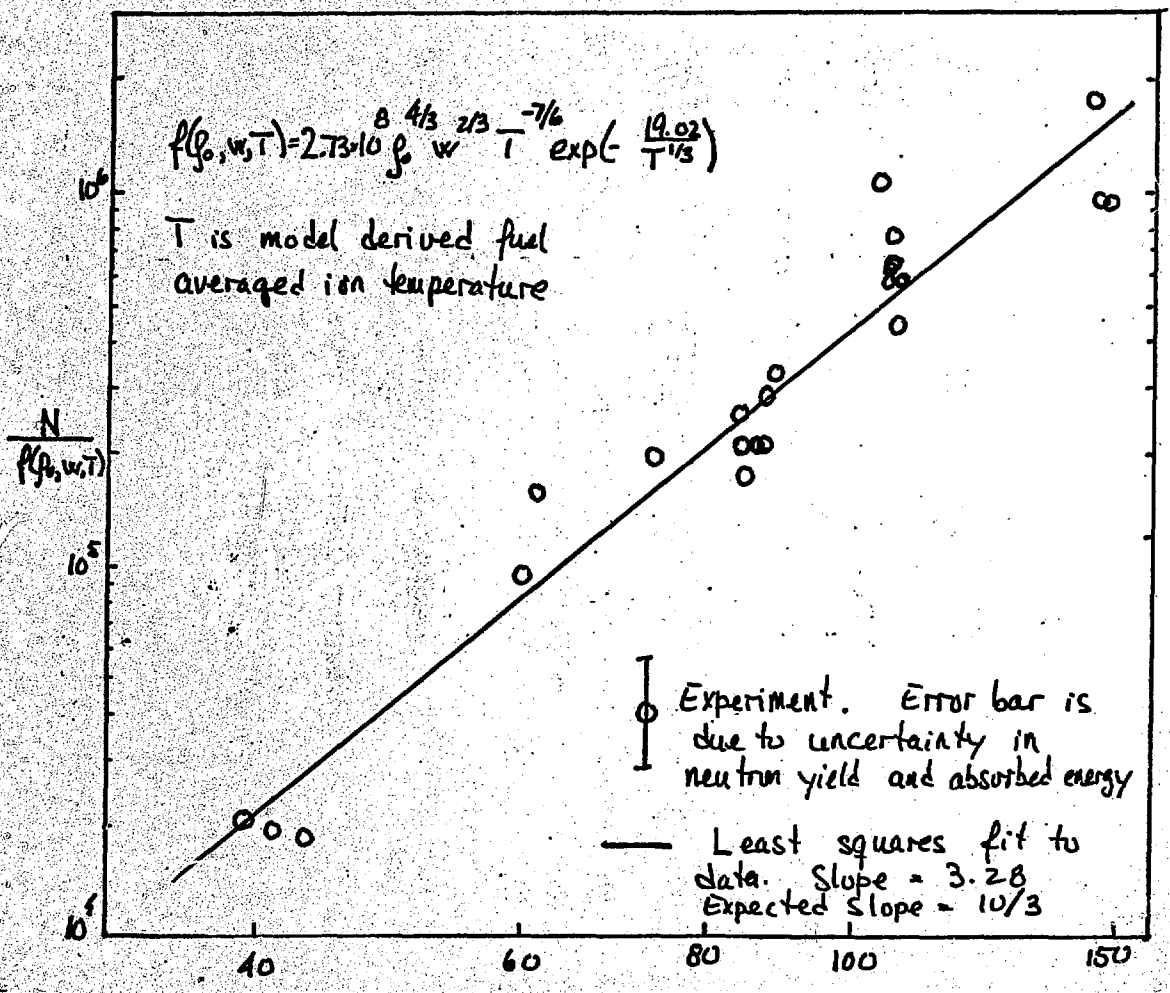

FIGURE 11

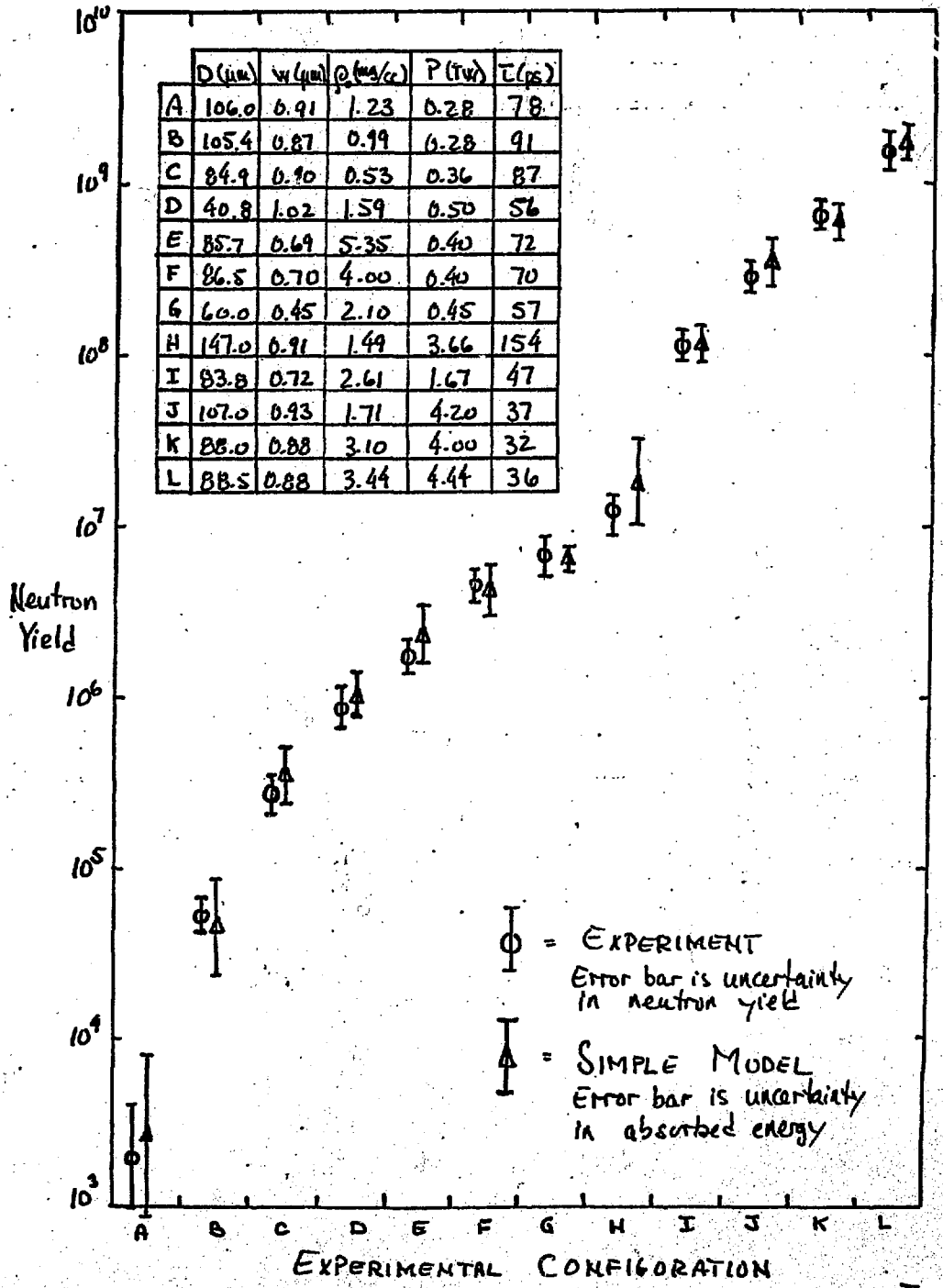

	D(μm)	w(μm)	ρ(mg/cc)	P(TW)	τ(ps)
A	106.0	0.91	1.23	0.28	78
B	105.4	0.87	0.99	0.28	91
C	84.9	0.90	0.53	0.36	87
D	40.8	1.02	1.59	0.50	56
E	85.7	0.69	5.35	0.40	72
F	86.5	0.70	4.00	0.40	70
G	60.0	0.45	2.10	0.45	57
H	147.0	0.91	1.49	3.66	154
I	83.8	0.72	2.61	1.67	47
J	107.0	0.93	1.71	4.20	37
K	88.0	0.88	3.10	4.00	32
L	88.5	0.88	3.44	4.44	36

FIGURE 12.

Neutron Yield vs Target Diameter

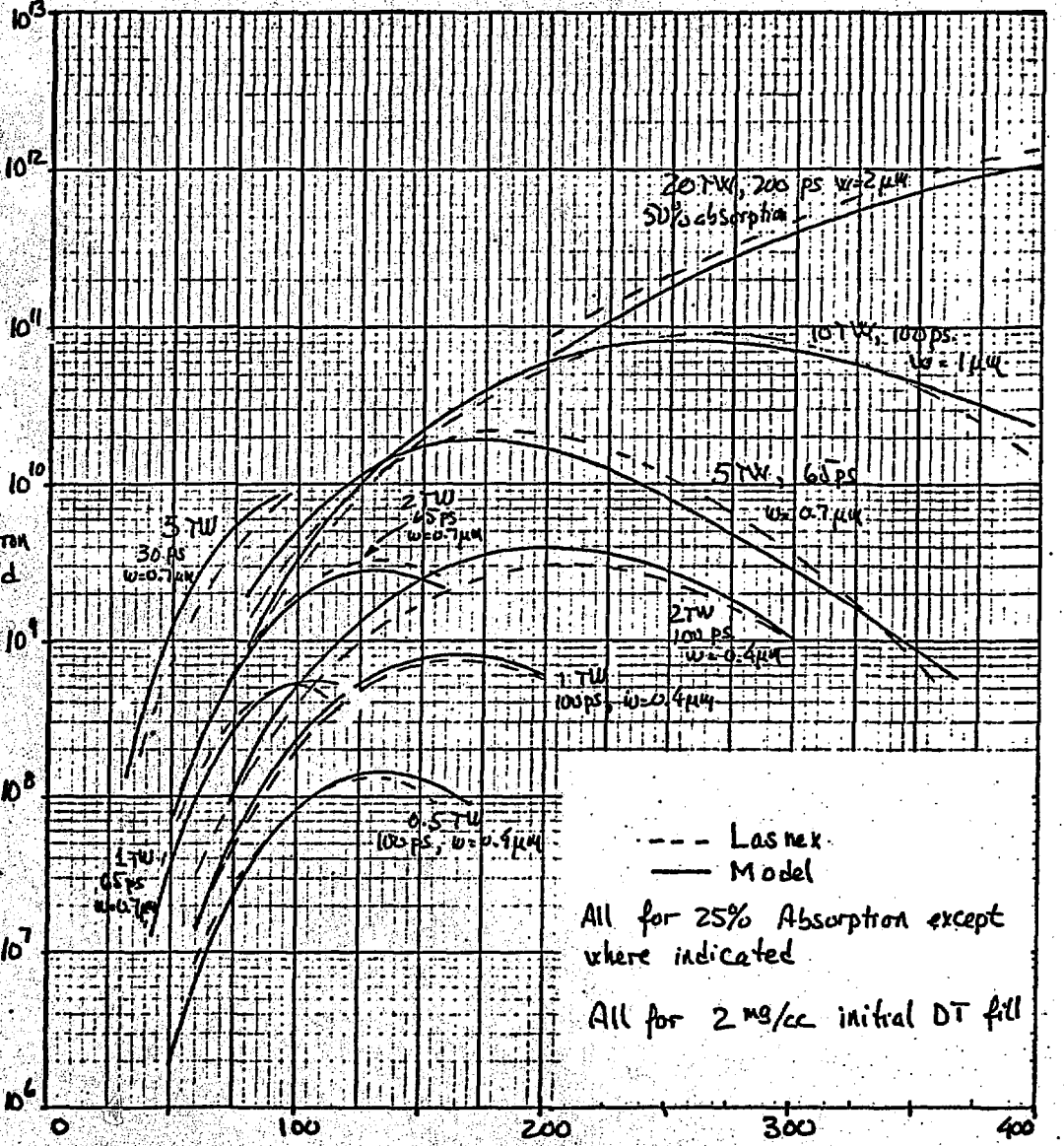

FIGURE 13

Neutron Yield vs Laser Pulselength

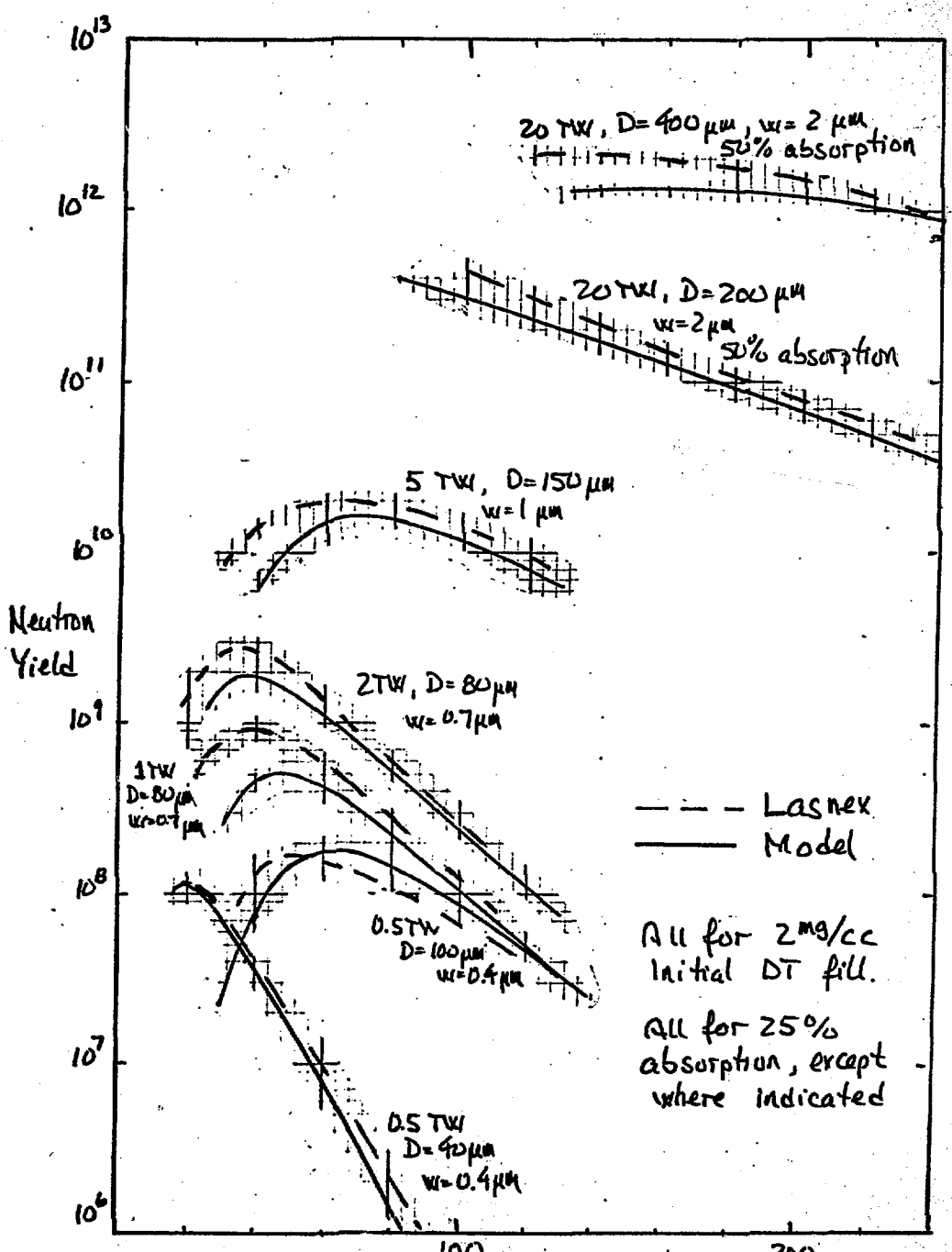

Figure 14

OPTIMUM TARGET DESIGNS AS A FUNCTION OF INCIDENT POWER

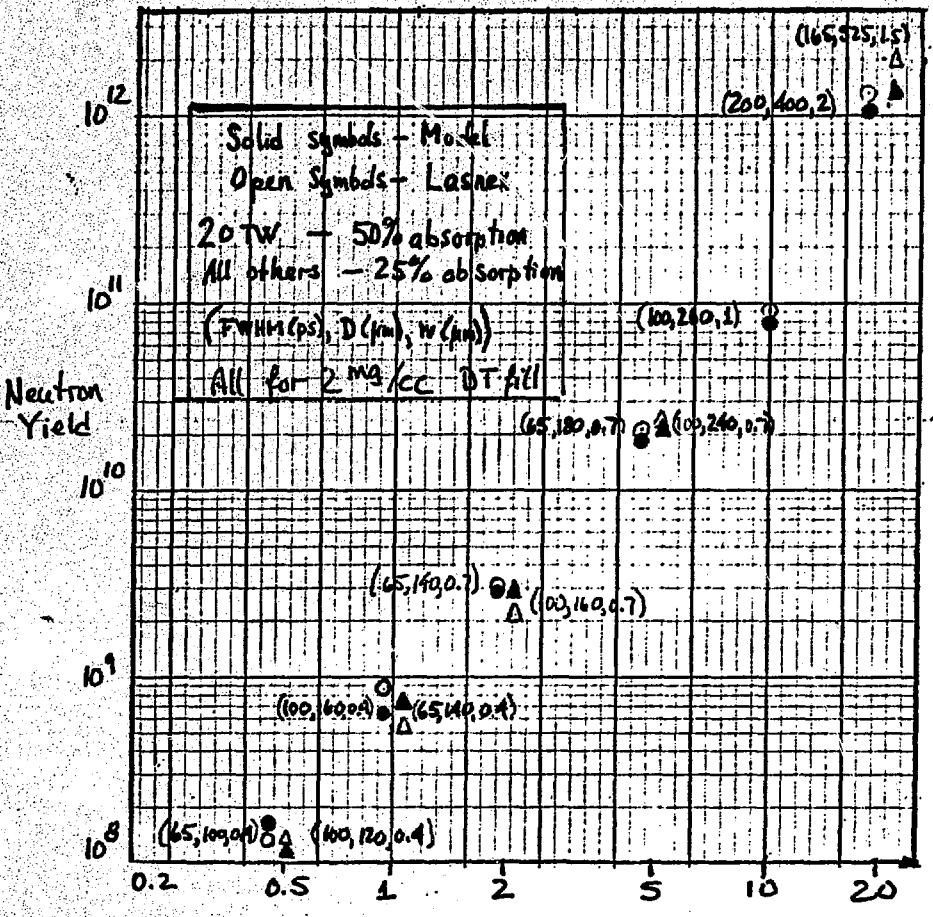

FIGURE 15

NEUTRON YIELD AND COMPRESSED DT DENSITY

FOR THICK-WALLED, LONG PULSE EXPLODING PUSHERS

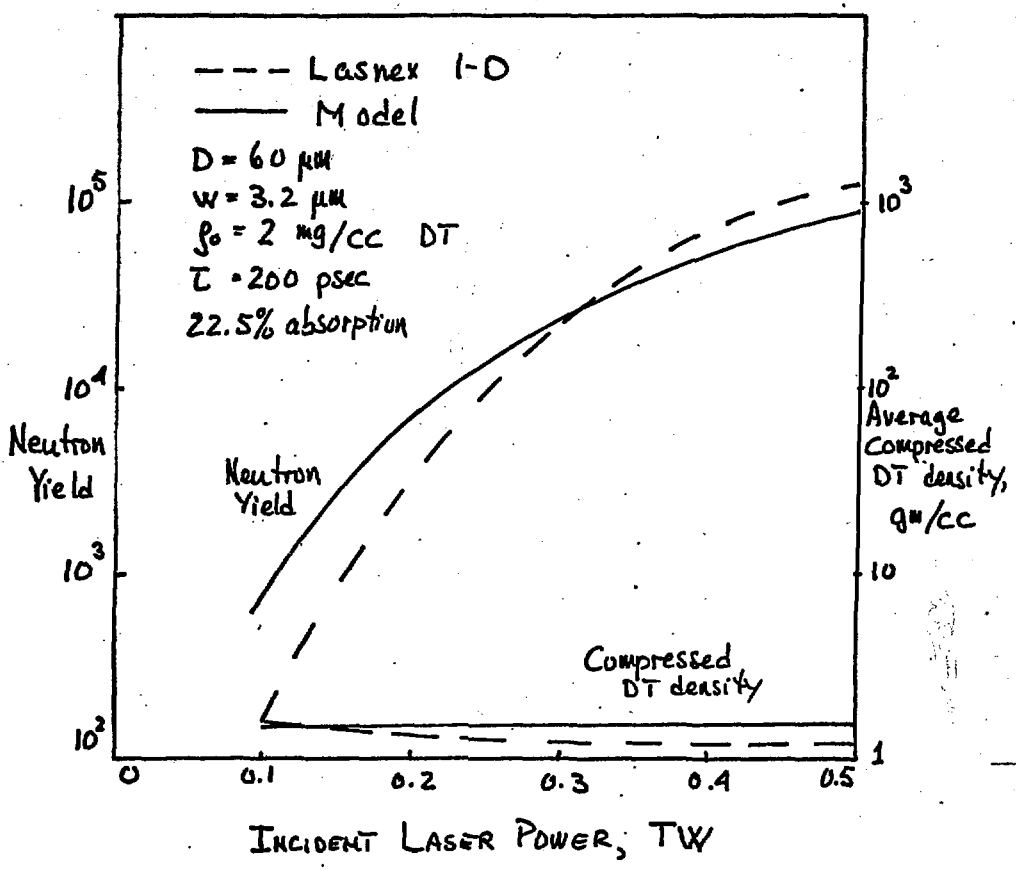

Figure 16

THE SIMPLE MODEL FAILS WHEN THERE IS A SIGNIFICANT MISMATCH BETWEEN τ AND THE IMPLOSION TIME

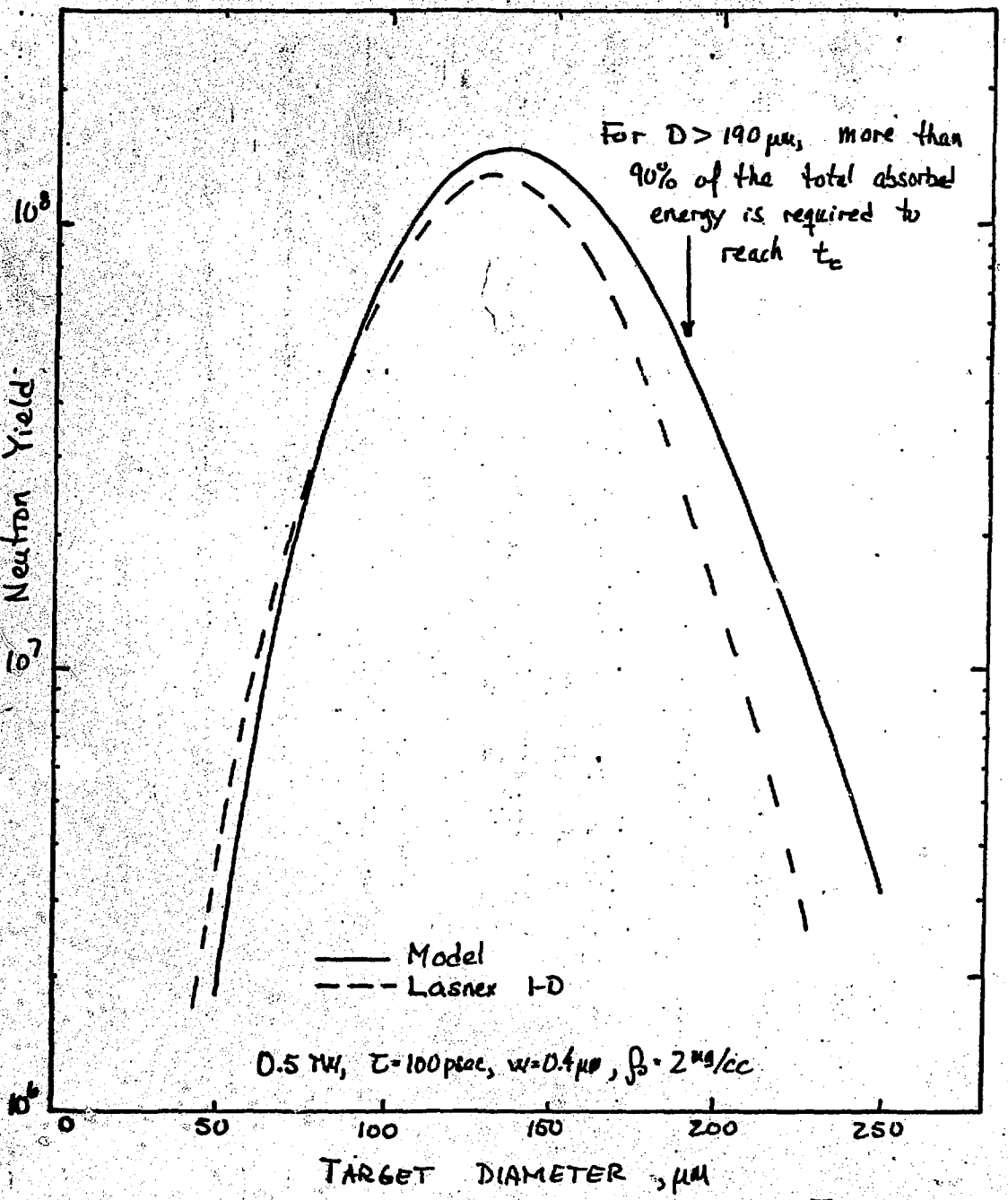

FIGURE 17a

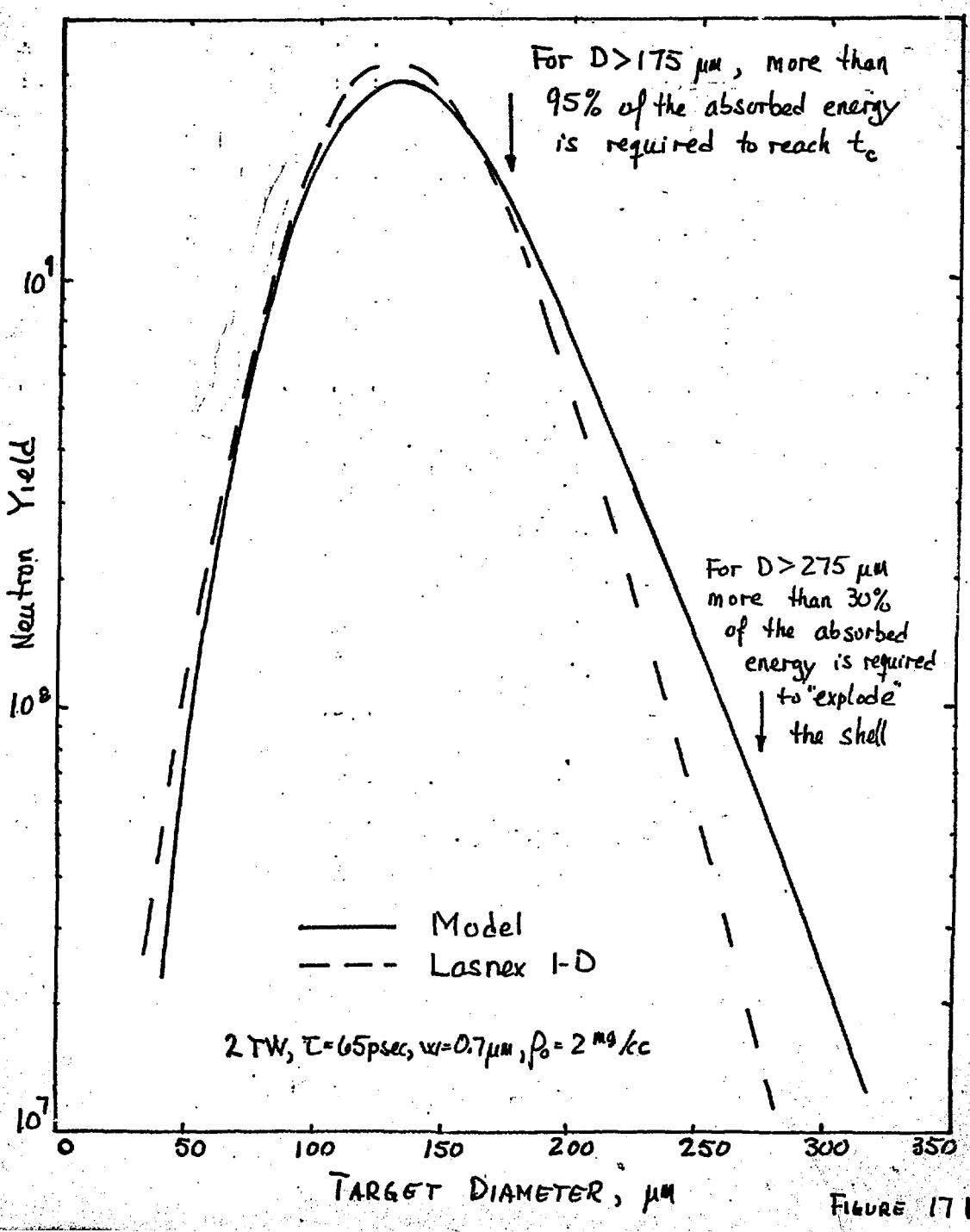
For D>175 μm, more than 95% of the absorbed energy is required to reach t_c
For D>275 μm more than 30% of the absorbed energy is required to "explode" the shell
Model
Lasnex 1-D
2 TW, τ=65psec, w=0.7μm, ρ_0=2 mg/cc
Neutron Yield
10^9
10^8
10^7
0
50
100
150
200
250
300
350
TARGET DIAMETER, μm

FIGURE 17b

FOR HIGH INTENSITY AND THIN-WALLED TARGETS, THE SUPERTHERMAL ELECTRONS ARE NOT EFFICIENTLY COUPLED TO THE SHELL

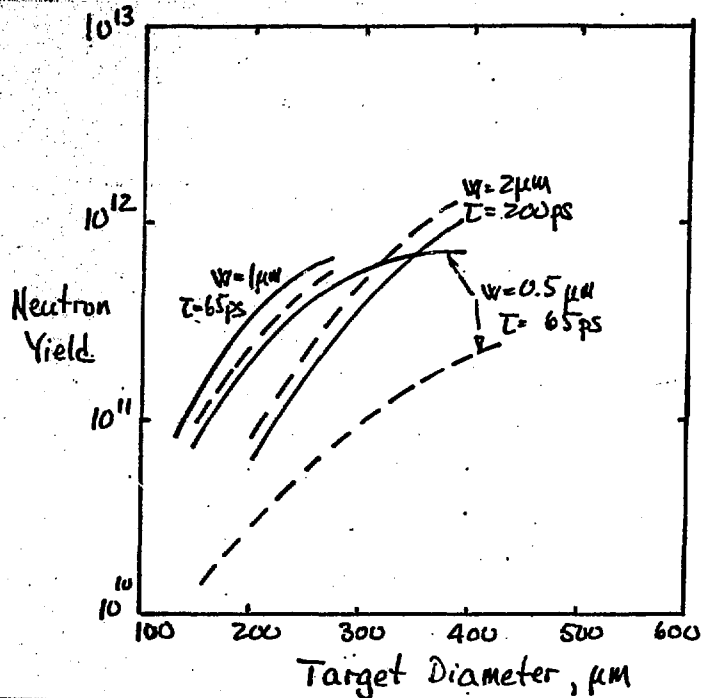

FIGURE 18